MTL TR 92-23

AD

AD-A251 448

NUMERICAL SIMULATION OF PERMEATION FROM DEPOSITED DROPLETS: MODEL EXPANSION

GERALDA SEVERE and JERRY H. MELDON
POLYMER RESEARCH BRANCH

April 1992

Approved for public release; distribution unlimited.

92-14996

US ARMY
LABORATORY COMMAND
MATERIALS TECHNOLOGY LABORATORY

U.S. ARMY MATERIALS TECHNOLOGY LABORATORY
Watertown, Massachusetts 02172-0001

92 6 08 013

UNCLASSIFIED

SECURITY CLASSIFICATION OF THIS PAGE (When Data Entered)

REPORT DOCUMENTATION PAGE		READ INSTRUCTIONS BEFORE COMPLETING FORM
1. REPORT NUMBER MTL TR 92-23	2. GOVT ACCESSION NO.	3. RECIPIENT'S CATALOG NUMBER
4. TITLE (and Subtitle) NUMERICAL SIMULATION OF PERMEATION FROM DEPOSITED DROPLETS: MODEL EXPANSION		5. TYPE OF REPORT & PERIOD COVERED Final Report
		6. PERFORMING ORG. REPORT NUMBER
7. AUTHOR(s) Geralda Severe and Jerry H. Meldon		8. CONTRACT OR GRANT NUMBER(s)
9. PERFORMING ORGANIZATION NAME AND ADDRESS U.S. Army Materials Technology Laboratory Watertown, Massachusetts 02172-0001 SLCMT-EMP		10. PROGRAM ELEMENT, PROJECT, TASK AREA & WORK UNIT NUMBERS D/A Project: 1L162105AH84
11. CONTROLLING OFFICE NAME AND ADDRESS U.S. Army Laboratory Command 2800 Powder Mill Road Adelphi, MD 20783-1145		12. REPORT DATE April 1992
		13. NUMBER OF PAGES 68
14. MONITORING AGENCY NAME & ADDRESS(if different from Controlling Office)		15. SECURITY CLASS. (of this report) Unclassified
		15a. DECLASSIFICATION/DOWNGRADING SCHEDULE

16. DISTRIBUTION STATEMENT (of this Report)

Approved for public release; distribution unlimited.

17. DISTRIBUTION STATEMENT (of the abstract entered in Block 20, if different from Report)

18. SUPPLEMENTARY NOTES

19. KEY WORDS (Continue on reverse side if necessary and identify by block number)

Mathematical model	Computer simulation
Barriers	Mass transfer
Flux (rate)	Diffusion coefficient

20. ABSTRACT (Continue on reverse side if necessary and identify by block number)

(SEE REVERSE SIDE)

DD FORM 1 JAN 73 1473 EDITION OF 1 NOV 65 IS OBSOLETE

UNCLASSIFIED

SECURITY CLASSIFICATION OF THIS PAGE (When Data Entered)

Block No. 20

ABSTRACT

A previously published model of permeation from a droplet has been expanded. Effects of downstream mass transfer resistance and concentration dependence of the diffusion coefficient have been included. An attempt was made to fit experimental results for the permeation of di-iso-propyl-methyl-phosphonate (DIMP) through Neoprene and natural rubber. Simulated data do not reproduce the initial pronounced delay of experimental permeation. Furthermore, no rationale has been identified for the anomalous dependence of "breakthrough time" upon barrier thickness observed with several experimental systems.

CONTENTS

	Page
INTRODUCTION	1
1.0 Mathematical Formulation	2
2.0 Results	6
3.0 Effect of the Contact Angle (θ)	12
4.0 Breakthrough Time Estimation	13
5.0 Conclusions	18
6.0 List of Notations	19
7.0 References	21
Appendix	
8.0 Conversion to Dimensionless Variables	23
9.0 Calculation of the Mass Transfer Coefficients	25
10.0 Finite-Difference Approximation	28
10.1 Boundary Conditions	29
11.0 One Dimensional Transport With Concentration Dependent Diffusion Coefficient	33
12.0 Programs Listing	41

INTRODUCTION

This report is a follow-up to " Numerical Simulation For The Permeation Of Barrier Materials By Neat Liquid Droplets " [1], which presented a solution to the governing differential equation using finite-difference methods (see also [2]). The focus there was upon the dependence of permeation rate on barrier thickness.

Theoretical results for the time dependence of penetrant fluxes were in qualitative agreement with experimental data obtained at an Army contract laboratory [3]. However, quantitative agreement was not always satisfactory. Consequently, a number of the simplifying assumptions upon which the model was based, are relaxed here in an attempt to identify the sources of discrepancy.

As described below, there is significant improvement in agreement between theory and experiment, when account is taken of the finite rate of penetrant transfer from the downstream barrier surface to the bulk sweep gas stream. This is primarily due to the low vapor pressures of chemical agent simulants, which minimize the driving forces for diffusion through the gas-phase boundary layer adjacent to the barrier.

Although near-quantitative agreement with experimental data is achieved in some cases by this change in boundary condition, there remain residual discrepancies in the earliest phase of an experimental run. Invariably, there is a pronounced delay in the experimental onset of permeation, which is inconsistent with the model's predictions. Attempts to replicate this behavior by varying the assumed droplet contact angle and penetrant diffusion coefficient, were unsuccessful.

The physical basis of the observed behavior, which remains unidentified, may also be the cause of a second, as yet inexplicable observation: the anomalous dependence of breakthrough time (t_B) upon barrier thickness (L). Theory predicts that t_B should vary as L^n, where $n \approx 2$. For some penetrant / barrier material combinations, n was found experimentally to be as great as 4 or 5. In the following report, the attempts to resolve these issues are described.

The model system considered here is the same. At time $\hat{t} = 0$, a pure droplet is placed upon an isotropic membrane in the form of a disc of radius $\hat{R}_s$ (see figure 1). The contact angle θ, made by the droplet with the surface, is assumed to remain constant as sorption proceeds and the droplet shrinks, while maintaining the shape of a spherical section. A non-permeating gas with zero penetrant concentration sweeps the barrier underneath. The gas above the barrier may also be flowing.

The dissolved penetrant attains the equilibrium concentration, $\hat{C}_i$, at the droplet base. Whereas the analysis in the previous report was based on the assumption of zero penetrant concentration in the bottom surface, $\hat{z} = \hat{L}$, in this report that assumption is relaxed. We instead examine the significance of the finite rate of mass transfer from barrier to sweep gas, and conclude that it can indeed be an important factor in the case of low vapor pressure penetrants.

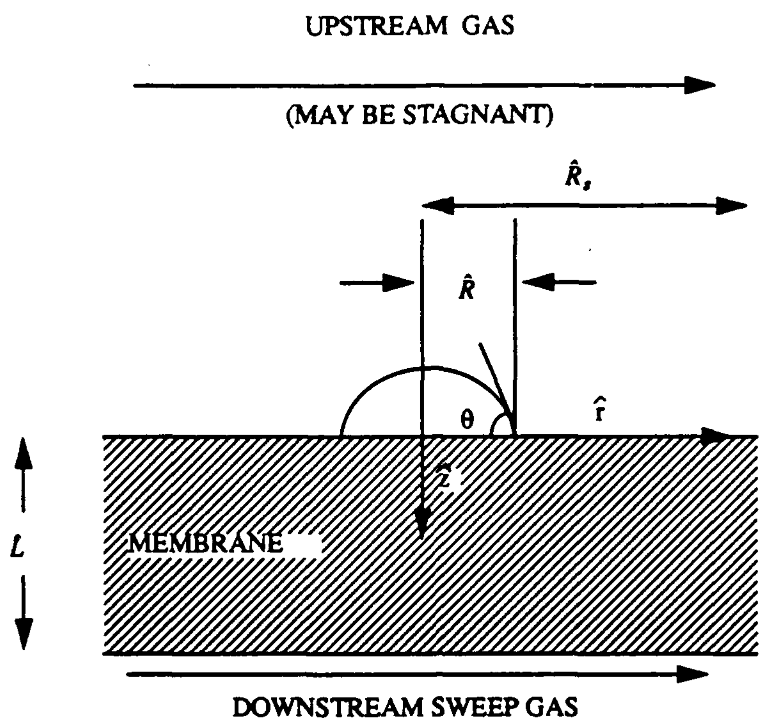

Figure 1. Schematic diagram of modelled system.

What follows are the mathematical formulation of the problem, an examination of the effects of finite mass transfer rates at the barrier surfaces, concentration dependence of the diffusion coefficient in the membrane, and the assumed value of θ, plus comparison with experimental results and predictions of the earlier model. A preliminary version of these results was presented at the November 1990 CRDEC Scientific Conference on Chemical Defense Research [4].

Previous work in this area also includes a substantial body of modelling by Frisch and coworkers [5, 6, 7, 8, 9], in which many of our observations regarding permeation behavior were independently made. However, these studies did not focus upon the issues addressed here.

1.0 Mathematical Formulation

Following the earlier model, we first neglect possible concentration dependence of the diffusion coefficient, $\hat{D}$. Thus, the concentration of penetrant in the membrane, $\hat{C}(\hat{r}, \hat{z}, \hat{t})$, is governed by the following equation in cylindrical coordinates:

$$\frac{\partial \hat{C}}{\partial \hat{t}} = \hat{D}\left(\frac{\partial^2 \hat{C}}{\partial \hat{r}^2} + \frac{1}{\hat{r}}\frac{\partial \hat{C}}{\partial \hat{r}} + \frac{\partial^2 \hat{C}}{\partial \hat{z}^2}\right) \tag{1}$$

subject to:

$$\hat{C}(\hat{r},\hat{z},0) = 0 \qquad 0 \le \hat{r} \le \hat{R}_s \qquad 0 \le \hat{z} \le \hat{L} \tag{2}$$

$$\hat{C}(\hat{r},0,\hat{t}) = \hat{C}_i \qquad 0 \le \hat{r} \le \hat{R}(\hat{t}) \qquad \hat{t} \ge 0 \tag{3}$$

$$\hat{D}\frac{\partial \hat{C}(\hat{r},0,\hat{t})}{\partial \hat{z}} = \hat{k}_m \hat{C}(\hat{r},0,\hat{t}) \qquad \hat{R}(\hat{t}) \le \hat{r} \le \hat{R}_s \qquad \hat{t} \ge 0 \tag{4}$$

$$-\hat{D}\frac{\partial \hat{C}(\hat{r},\hat{L},\hat{t})}{\partial \hat{z}} = \hat{k}_s \hat{C}(\hat{r},\hat{L},\hat{t}) \qquad 0 \le \hat{r} \le \hat{R}_s \qquad \hat{t} \ge 0 \tag{5}$$

$$\frac{\partial \hat{C}(\hat{R}_s,\hat{z},\hat{t})}{\partial \hat{r}} = 0 \qquad 0 \le \hat{z} \le \hat{L} \qquad \hat{t} \ge 0 \tag{6}$$

$$\frac{\partial \hat{C}(0,\hat{z},\hat{t})}{\partial \hat{r}} = 0 \qquad 0 \le \hat{z} \le \hat{L} \qquad \hat{t} \ge 0 \tag{7}$$

The caret (^) is used to distinguish the above quantities from the dimensionless ones defined below.

The $\hat{k}_m$ in equation (4) is an effective mass transfer coefficient representing convection from the upstream barrier surface. Correspondingly, the $\hat{k}_s$ in equation (5) is the coefficient governing mass transfer from the downstream barrier surface to the sweep gas. The term $\hat{R}_s$ can be taken to denote either the membrane's radius or, in the case of a regularly spaced array of droplets, the symmetry radius around each droplet (see figure 2).

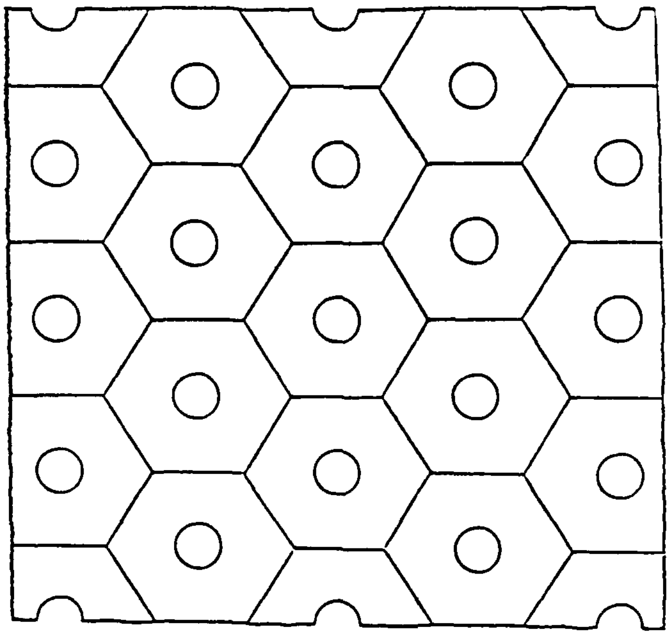

Figure 2. Face view of barrier showing a symmetric array of droplets. Hexagons indicate locus of symmetry around each droplet.

In addition to equation (1), auxiliary relationships relate the time-varying droplet radius, $\hat{R}(\hat{t})$, to droplet mass losses by transfer into the barrier and upstream gas. Thus:

$$\hat{\rho}(\hat{V}_0 - \hat{V}) = \hat{q}_B + \hat{q}_E \tag{8}$$

where:

$\hat{\rho}$ is droplet density and $\hat{V}$ its volume, which is related to $\hat{R}$ by:

$$\hat{V}(\hat{t}) = \frac{\pi}{3}\hat{R}^3(\hat{t})\, g(\theta) \tag{9}$$

and

$$g(\theta) = \frac{\sin\theta\,(2+\cos\theta)}{(1+\cos\theta)^2} \tag{10}$$

($\hat{V}_0$ is the initial droplet volume; $\hat{R}_0$ is the initial $\hat{R}$ value.)

The cumulative mass flow into the membrane at the base of the droplet, $\hat{q}_B$, is given by:

$$\hat{q}_B = -2\pi\hat{D}\int_0^{\hat{t}}\int_0^{\hat{R}(\hat{t})} \frac{\partial\hat{C}(\hat{r},0,\hat{t})}{\partial\hat{z}}\hat{r}\,d\hat{r}\,d\hat{t} \tag{11}$$

and the mass evaporated from the surface of the droplet, $\hat{q}_E$, is given by:

$$\hat{q}_E = \hat{k}_d\hat{C}_e^V\int_0^{\hat{t}}\hat{A}(\hat{t})\,d\hat{t} \tag{12}$$

where $\hat{C}_e^V = \frac{\hat{P}^V}{RT}$, $\hat{P}^V$ = vapor pressure, $\hat{k}_d$ is the effective mass transfer coefficient for evaporation, and the exposed droplet surface area is given by:

$$\hat{A}(\hat{t}) = \pi\hat{R}^2(\hat{t})\, g(\theta) \tag{13}$$

The above relationships must be solved simultaneously to determine the droplet radius and concentrations inside the barrier versus time. Once the concentrations are determined, it is possible to calculate the amount permeated through the downstream surface, ($\hat{q}_P$) and the amount evaporated from the unwet portion of the upstream membrane surface ($\hat{q}_M$) and the amount accumulated within the barrier ($\hat{q}_A$) from:

$$\hat{q}_P = 2\pi\hat{k}_s\int_0^{\hat{t}}\int_0^{\hat{R}_*}\hat{C}(\hat{r},\hat{L},\hat{t})\,\hat{r}\,d\hat{r}\,d\hat{t} \tag{14}$$

$$\hat{q}_M = 2\pi\hat{k}_m\int_0^{\hat{t}}\int_{\hat{R}(\hat{t})}^{\hat{R}_*}\hat{C}^V(\hat{r},\hat{t})\,\hat{r}\,d\hat{r}\,d\hat{t} \tag{15}$$

The concentration of penetrant vapor in equilibrium with the local dissolved concentration in the top surface, is calculated from:

$$\hat{C}^{V}(\hat{r},\hat{t}) = \frac{\hat{C}(\hat{r},0,\hat{t})}{\hat{C}_i}\hat{C}_e^{V} \tag{16}$$

The implicitly linear relationship between equilibrium gas and polymer phase concentrations is an approximation made in the absence of further data.

In addition, the amount accumulated within the barrier is calculated from:

$$\hat{q}_A = 2\pi\int_0^L\int_0^{\hat{R}_s}\hat{C}(\hat{r},\hat{z},\hat{t})\,\hat{r}\,d\hat{r}\,d\hat{z} \tag{17}$$

As an internal check on the solution, it must be true that:

$$\hat{q}_B = \hat{q}_A + \hat{q}_P + \hat{q}_M \tag{18}$$

The solution is outlined in the appendix. Significantly, the behavior of the system is governed by the following set of dimensionless parameters:

$$\theta \tag{19}$$

$$\sigma = \frac{\hat{C}_i}{\hat{\rho}} \tag{20}$$

$$\lambda = \hat{L}/\hat{R}_0 \tag{21}$$

$$R_s = \frac{\hat{R}_s}{\hat{R}_0} \tag{22}$$

$$k_s = \frac{\hat{k}_s\hat{L}}{\hat{D}} \tag{23}$$

$$k_d = \frac{\hat{k}_d\hat{C}_e^{V}\hat{L}}{\hat{D}\hat{C}_i} \tag{24}$$

$$k_m = \frac{\hat{k}_m\hat{C}_e^{V}\hat{L}}{\hat{D}\hat{C}_i} \tag{25}$$

2.0 Results.

To validate our numerical model, we compared its predictions with experimental data obtained several years ago at Southern Research Institute, in particular that obtained using two membrane materials, Neoprene and natural rubber [3]. A 5 μl droplet of diisopropyl methyl phosphonate (DIMP) was deposited onto 10 cm^2 membranes of various thicknesses. In most experiments, both surfaces of the membrane were exposed to an air flow of 1 liter/min. However, in some cases there was no air flow above the barrier.

As in the previous report [1], a contact angle of 60^0 was assumed in the absence of a measured value, which leads to estimates of 0.171 cm for $\hat{R}_0$ and of 10.44 for R_s. On the basis of separate immersion experiments [10], the diffusion coefficients, $\hat{D}$, of DIMP in Neoprene and natural rubber were estimated at 7.6×10^{-8} cm^2/sec and 7.8×10^{-8} cm^2/sec, respectively. Furthermore, based on the droplet density, $\hat{\rho}$, of 0.98 g/cm^3 and measured solubilities, $\hat{C}_i$, we calculated the partition coefficient, σ, (the ratio of $\hat{C}_i$ to $\hat{\rho}$) to equal 0.43 for Neoprene and 0.20 for natural rubber.

The dimensionless mass transfer coefficients at the bottom surface, k_s were estimated (see appendix) at 0.94 and 1.83 for Neoprene membranes 5.6×10^{-2} and 1.09×10^{-1} cm thick, respectively. The corresponding values for natural rubber were 1.80 and 3.47 for 5.23×10^{-2} and 1.01×10^{-1} cm thicknesses, respectively. For the experiments performed without air flow above the barrier - that is, with a sealed upper chamber - parameters k_m and k_d were set at zero, since the amount of DIMP vapor required to saturate the chamber represented a negligible fraction of initial droplet mass (see appendix). Based on these conditions, and the above (R_s, θ, σ) values, the theoretical curves in figures 3 through 6 were generated for comparison with experiment.

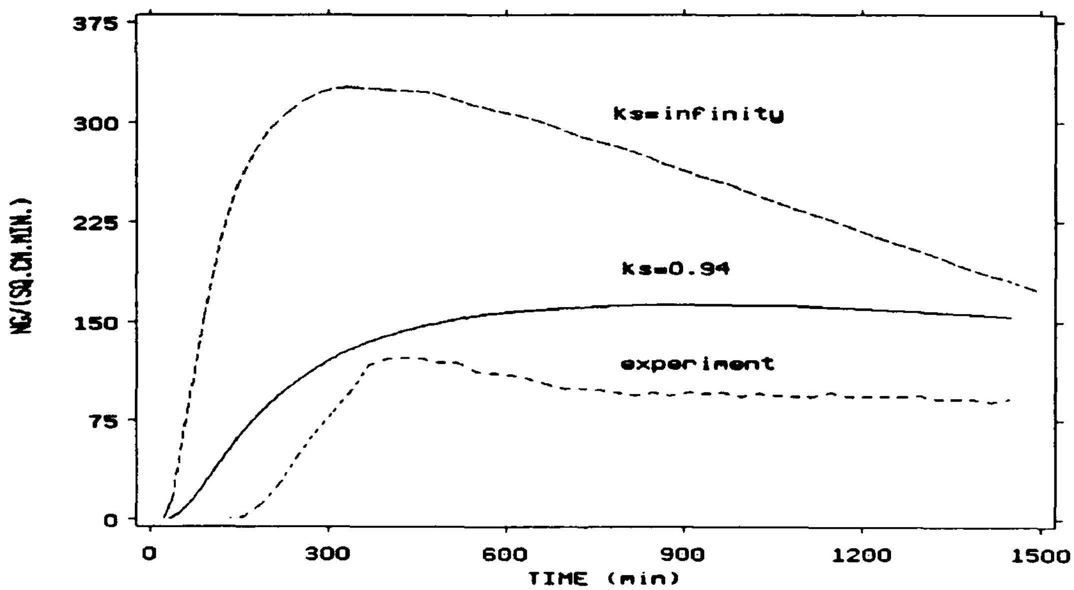

Figure 3. DIMP permeation rate vs. time for a Neoprene membrane. $L = 5.23 \times 10^{-2}$ cm; $k_m = k_d = 0$

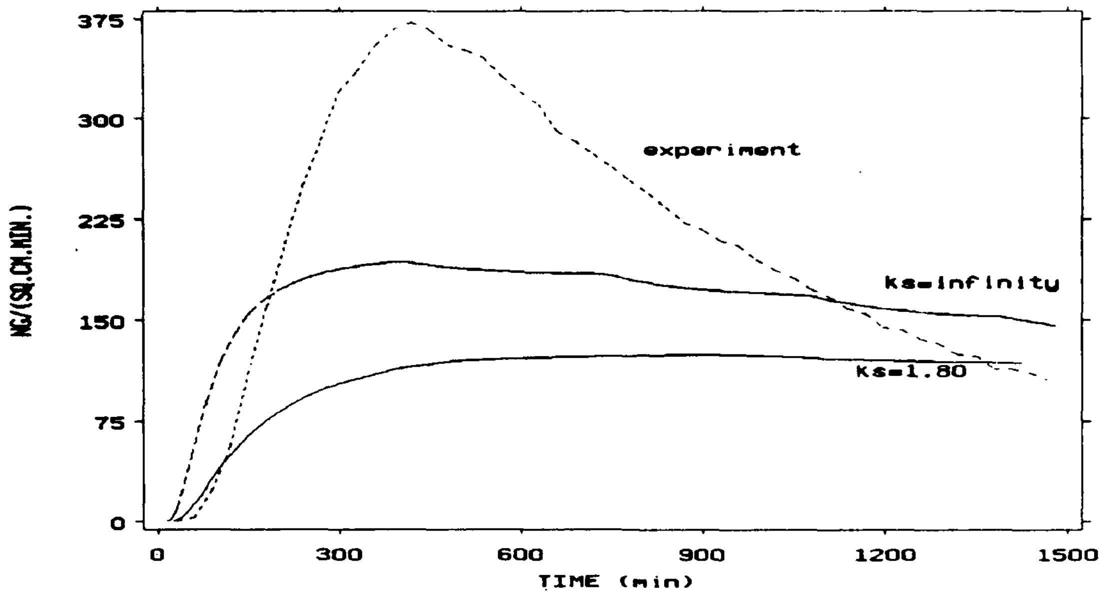

Figure 4. DIMP permeation rate vs. time for a natural rubber membrane. $L = 5.23 \times 10^{-2}$ cm; $k_m = k_d = 0$

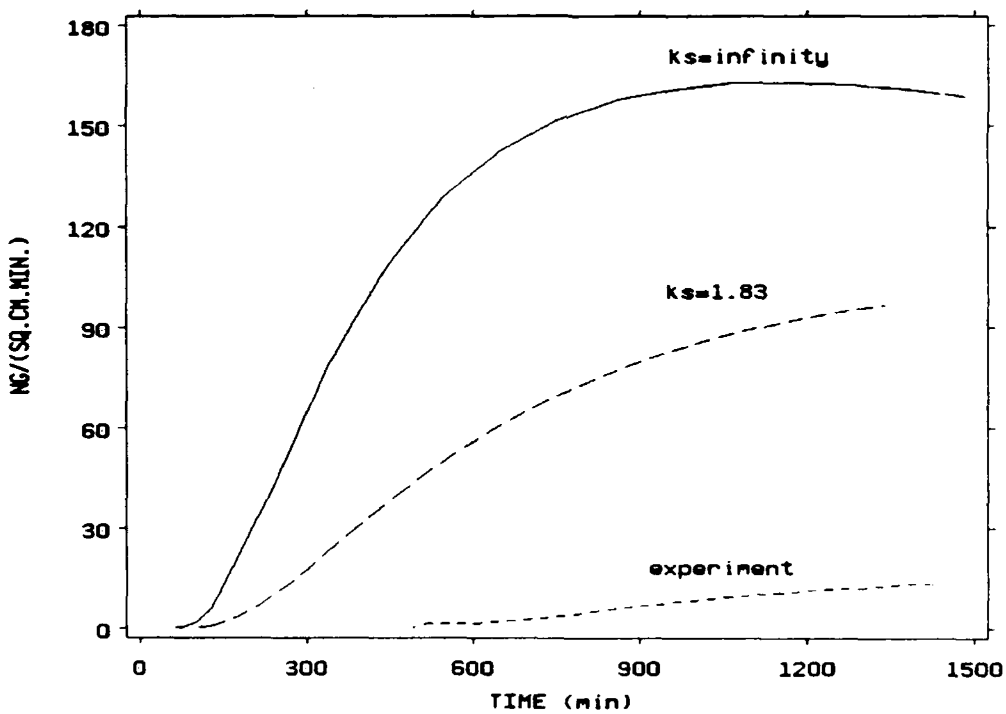

Figure 5. DIMP permeation rate vs. time for Neoprene membrane. $L = 1.09 \times 10^{-1}$ cm; $k_m = k_d = 0$

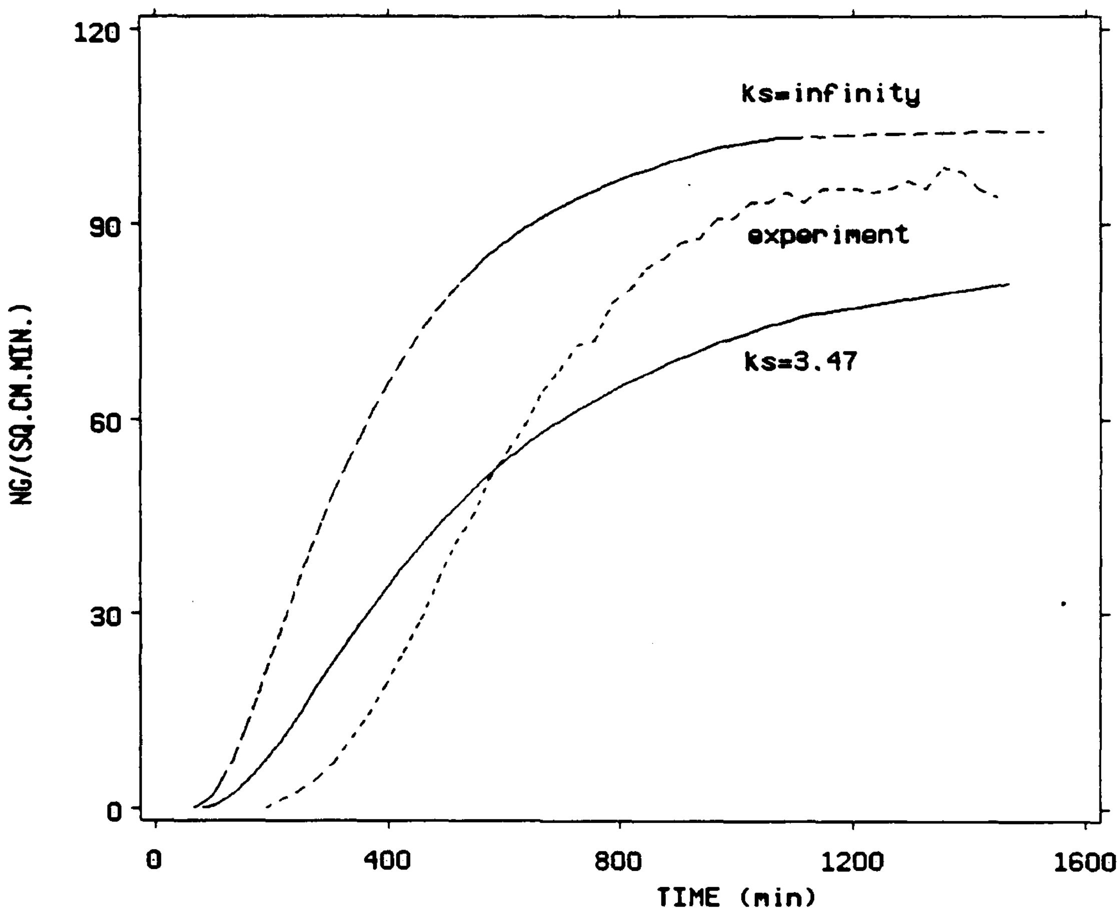

Figure 6. DIMP permeation rate vs. time for a natural rubber membrane. $\hat{L} = 1.01 \times 10^{-1}$ cm; $k_m = k_d = 0$

For both thicknesses and both materials the computer- generated curves do not show the pronounced delay observed at the beginning of the experimental curves. In addition, calculated fluxes do not exhibit the maxima measured in the cases of thinner barriers (see figure 4). Included in each figure are curves generated from the earlier model [1], marked "$k_s = \infty$", which neglected the downstream mass transfer resistance of the sweep-gas boundary layer and, accordingly, set $\hat{C} = 0$ at $\hat{z} = \hat{L}$. The results in figures 3-6 suggest that fluxes were, in fact, limited somewhat by this resistance.

We attempted to improve the fit to the Neoprene data by varying $\hat{D}$ by a factor of three higher and lower (see figures 7 and 8; note: this caused k_s to vary inversely by the same factor). As expected, permeation rates increased as $\hat{D}$ increased and initial lag time shortened as $\hat{D}$ increased. Significantly, decreasing $\hat{D}$ improved substantially the fit to the early and long-time flux data for both thicknesses. Nontheless, manipulation of $\hat{D}$ alone is insufficient to replicate the shape of the flux curve, including a maximum, for both cases. Furthermore, it is apparent in figures 4 and 6 that similar adjustements in $\hat{D}$ cannot substantially improve the fit to the data for natural rubber.

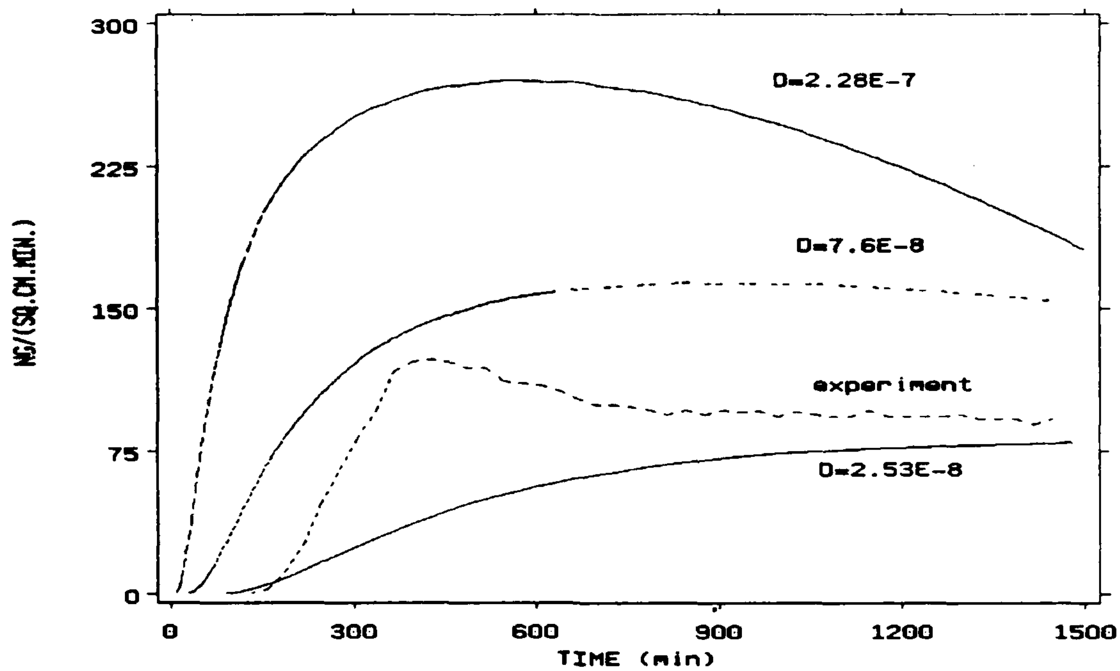

Figure 7. DIMP permeation rate vs. time for Neoprene membrane. $\hat{L}$= $5.6x10^{-2}$ cm; k_m=k_d=0; sensitivity to assumed value of $\hat{D}$.

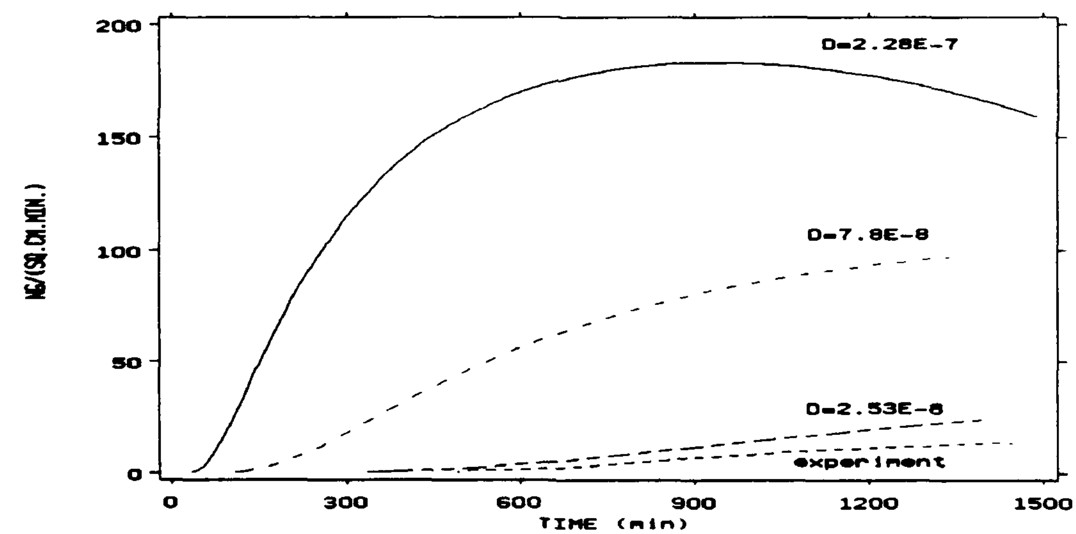

Figure 8. DIMP permeation rate vs. time for Neoprene membrane. $\hat{L}$= 1.09 $x10^{-1}$ cm; k_m=k_d=0;sensitivity to assumed value of $\hat{D}$.

Next, the diffusion coefficient was held constant while varying the downstream mass transfer coefficient, $\hat{k}_s$, by the same factors (thereby multiplying k_s by the same factors as well; see figures 9 and 10). Again as expected, increasing the mass transfer coefficient increases the flux. However, varying $\hat{k}_s$ from its estimated value has no substantial effect on the permeation time lag. On the other hand, decreasing it improves the fit between theory and experiment, for the long-time fluxes. It appears that manipulation of $\hat{D}$ and/or $\hat{k}_s$ alone cannot yield quantitative agreement with the data for both thicknesses of Neoprene.

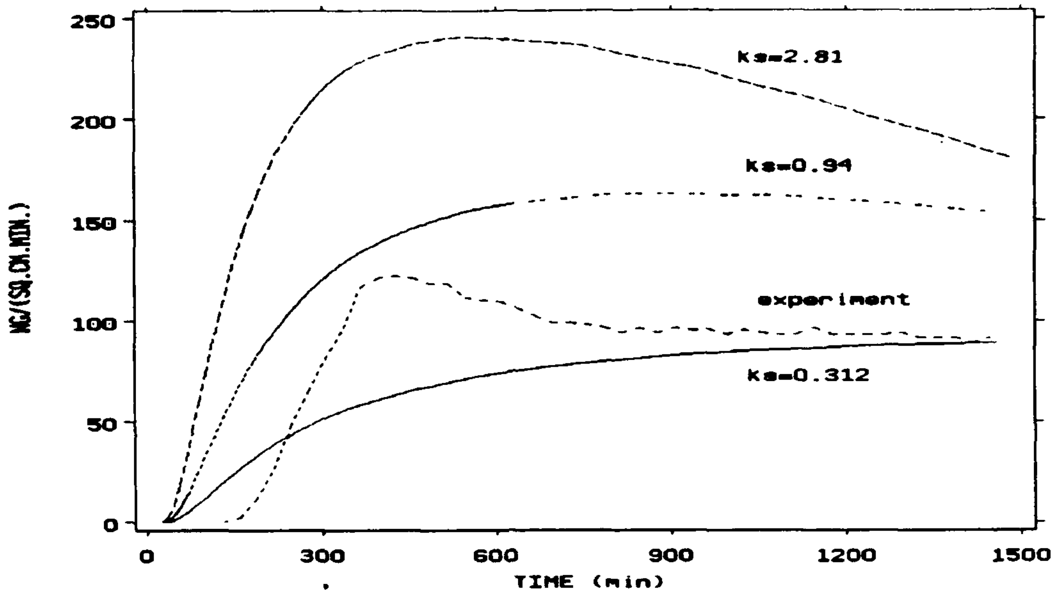

Figure 9. DIMP permeation rate vs. time for Neoprene membrane. $L = 5.6 \times 10^{-2}$ cm; $k_m = k_d = 0$; sensitivity to assumed value of $\hat{k}_s$.

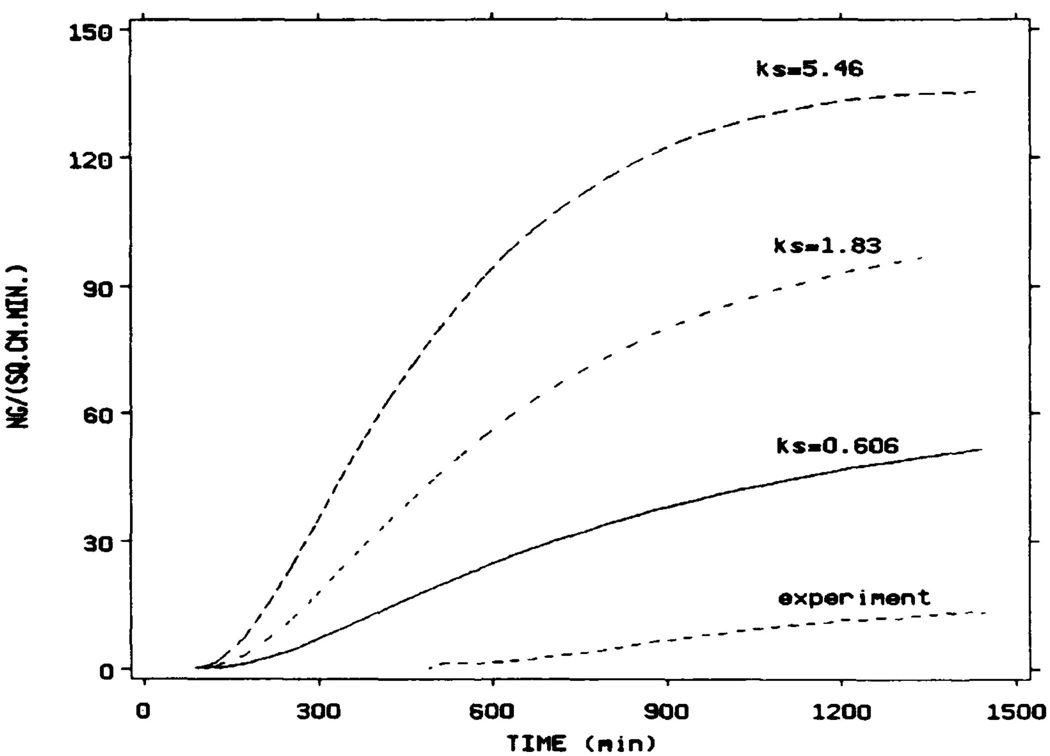

Figure 10. DIMP permeation rate vs. time for Neoprene membrane. $L = 1.09 \times 10^{-1}$ cm; $k_m = k_d = 0$; sensitivity to assumed value of $\hat{k}_s$.

Finally, we modelled cases in which evaporation from the droplet and upstream barrier surface is not negligible, i.e., where air flows at 1 L/min through the upper chamber. Values for the mass transfer coefficient, k_m, estimated as described in the appendix, were 2.52 for 1.02×10^{-1} cm thick natural rubber and 1.34 for 1.09×10^{-1} cm thick Neoprene. Then, with the previously estimated parameters and the estimated k_m and k_d values, the curves shown in figures 11 and 12 were obtained. Comparison of the experimental curves in figures 6 and 12 reveals the pronounced effect of upstream evaporation losses in the case of natural rubber. (The effect in the case of Neoprene is not as easily identified by comparison of the experimental curves in figures 5 and 11, but is of similar magnitude.) The theoretically calculated effects of evaporation from the droplet and unwet portion of the upstream surface are small compared to the effect of downstream gas-phase mass transfer resistance. Much higher evaporation rates are necessary to conform theory to experiment.

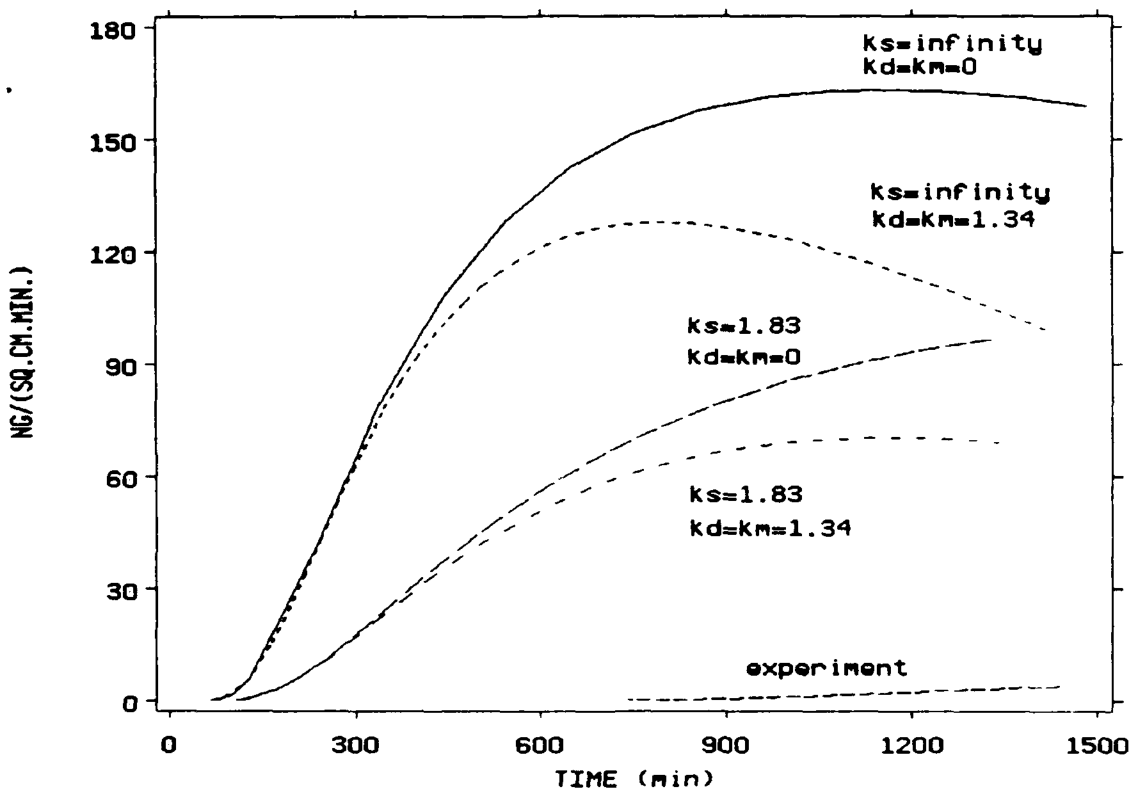

Figure 11. DIMP permeation rate vs. time for Neoprene membrane. $L=1.09 \times 10^{-1}$ cm. Experiment with 1 L/min air flow in both the upper and lower chambers of the test cell. Sensitivity to assumed gas-phase mass transfer coefficients.

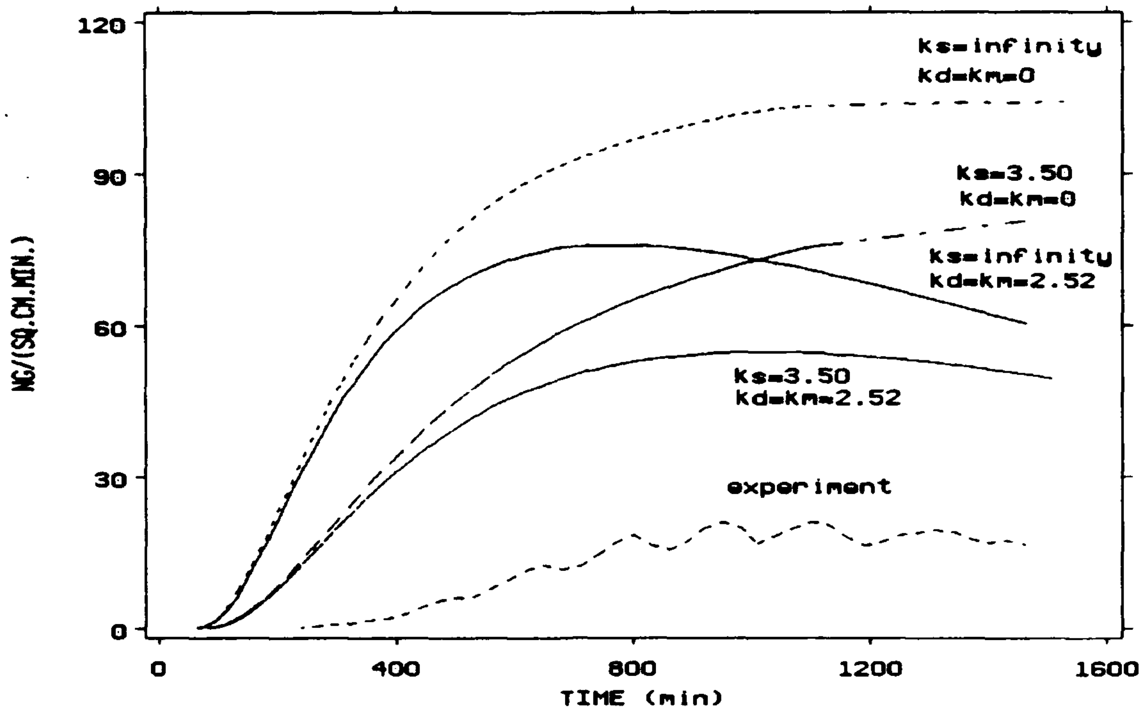

Figure 12. DIMP permeation rate vs. time for Natural rubber membrane. L=1.02 x 10^{-1} cm. Experiment with 1 L/min air flow in both the upper and lower chambers of the test cell. Sensitivity to assumed gas-phase mass transfer coefficients.

3.0 Effect of the Contact Angle (θ)

We examined the sensitivity to contact angle, of the permeation rate of DIMP through a 5.61 x 10^{-2} cm Neoprene membrane. To do so, we replaced the 60^0 value of θ in equation (10) with respective values of 30^0 and 90^0. This affected not only the initial droplet radius ($\hat{R}_0$), but also the wetted area throughout a simulated run. The resulting values for $\hat{R}_0$, R_s and λ, respectively, were 0.226 cm, 7.88 and 0.25 when θ was 30^0; and 0.13 cm, 13.73 and 0.43 when θ was 90^0. Calculated permeation rate curves for the three contact angles and the experimental curve are shown in figure 13. Permeation accelerates as θ decreases, because of the correspondingly greater wetted areas. No assumed angle yields a good overall fit. Variation of θ had, understandably, no effect on the delay in the onset of permeation.

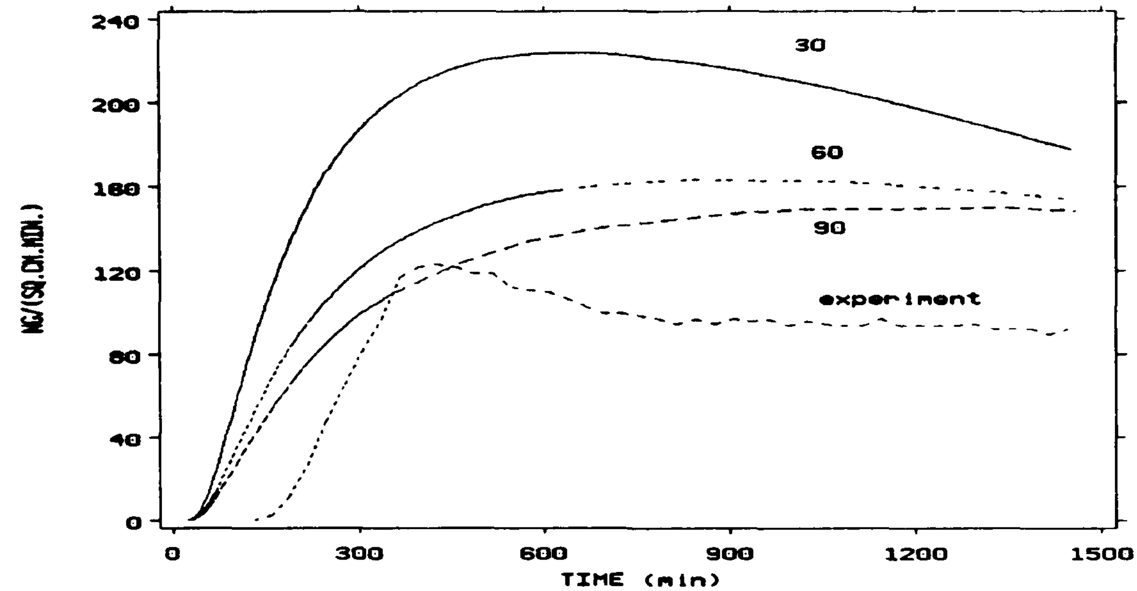

Figure 13. DIMP permeation rate vs. time for a Neoprene membrane: $L = 5.61 \times 10^{-2}$ cm; $k_m = k_d = 0$; $k_s = 0.94$; $\sigma = 0.43$. Numerical label denotes value of θ.

4.0 Breakthrough Time Estimation

In order to further investigate the early time behavior, we developed an analysis in which allowance was made for dependence of the diffusion coefficient on concentration of penetrant. This was undertaken based on the presumption that a substantially lower diffusion coefficient near $\hat{z} = L$, at the start of an experiment, might explain the consistently observed lag in the onset of permeation.

It had been concluded in the earlier report [1], that theoretically calculated early time permeation behavior is frequently indistinguishable from that with a fully wetted surface. This observation allowed us to explore the ramifications of a variable diffusion coefficient (which complicates the mathematics) in the context of a single spatial dimension (which requires much less computer time than the 2-dimensional model deployed until now). The surface area used to calculate amount permeated was that of the initial droplet/barrier interface.

We again assume a barrier of thickness L whose lower surface is swept by a gas with zero bulk penetrant concentration. However, the upper surface at $\hat{z} = 0$ is now completely covered with penetrant and remains so throughout an experiment (see figure 14).

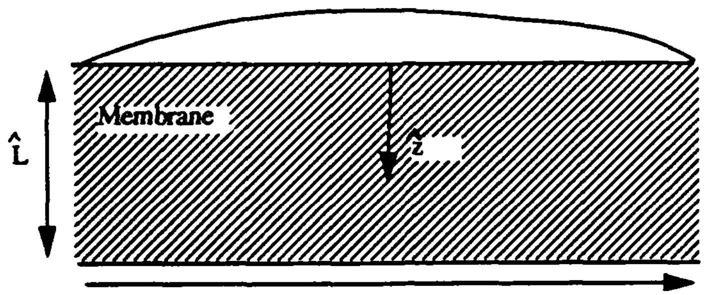

Figure 14. Schematic representation of model with fully wetted surface.

The governing partial differential equation becomes:

$$\frac{\partial \hat{C}}{\partial \hat{t}} = \hat{D}\frac{\partial^2 \hat{C}}{\partial \hat{z}^2} + \left(\frac{\partial \hat{D}}{\partial \hat{C}}\right)\left(\frac{\partial \hat{C}}{\partial \hat{z}}\right)^2 \tag{26}$$

and the boundary and initial conditions reduce to:

$$\hat{C} = 0 \qquad \hat{t} < 0 \qquad 0 \le \hat{z} \le \hat{L} \tag{27}$$

$$\hat{C} = \hat{C}_i \qquad \hat{t} \ge 0 \qquad \hat{z} = 0 \tag{28}$$

$$-\hat{D}(\hat{C})\frac{\partial \hat{C}}{\partial \hat{z}} = \hat{k}_s \hat{C} \qquad \hat{t} \ge 0 \qquad \hat{z} = \hat{L} \tag{29}$$

In addition, we adopt an expression for the concentration dependence of the diffusion coefficient which has conventionally been applied to modelling of diffusion in polymers [11]:

$$\hat{D}(\hat{C}) = \hat{D}_0 e^{m(\hat{C}/\hat{C}_i)} \tag{30}$$

where m is a constant characteristic of the polymer/solvent pair. A description of the finite-difference method used to solve for concentrations and amount permeated is presented in the appendix.

To verify the accuracy of our simulation, we compared the amount permeated at anytime in the limiting case when $\hat{D}$ is constant (m=0), with results obtained from a closed-form solution for the mathematically analogous problem of conduction of heat in a slab, with constant thermal diffusivity [12]. We also compared steady-state concentration profiles obtained from: (a) the solution to (26) with the time derivative set at zero, which collapses to: $\frac{d}{d\hat{z}}\left(\hat{D}\frac{d\hat{C}}{d\hat{z}}\right) = 0$; and (b) the long-time behavior of the solution to (26) (i.e., at sufficiently long times that concentrations are no longer changing).

Figure 15 depicts typical results for dimensionless concentration versus dimensionless position. The parameters correspond to a fully wetted membrane with 2.54×10^{-2} cm (10 mils) thick, and with a 1 liter/min sweep gas flow in the lower surface of the membrane. The results from the two numerical solutions (steady-state and transient) overlap, as shown for both m=1 and m=10. Furthermore, because of the comparatively low estimated value of k_s (when m=1), external mass transfer (from the downstream surface to the bulk sweep gas) is permeation-rate-limiting, as indicated by the high steady-state dimensionless concentration, C, at z=1 (i.e., most of the overall chemical potential driving force is dissipated in the gas, not the membrane phase).

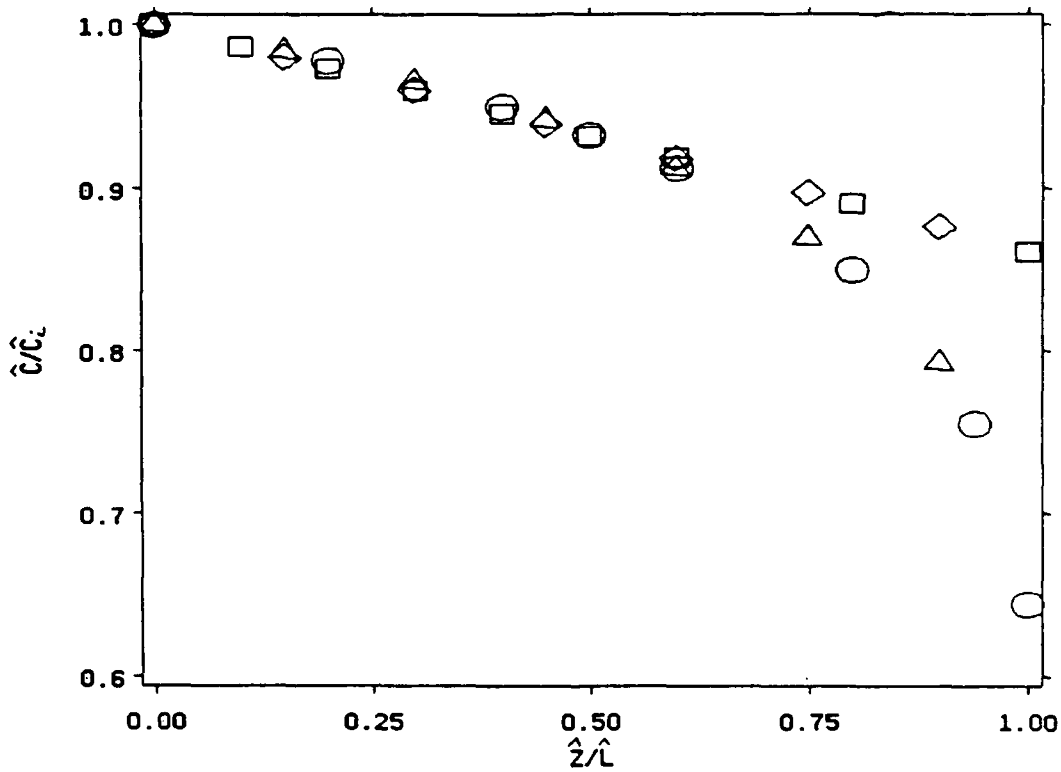

Figure 15. Steady-state dimensionless concentration profiles with concentration dependent diffusion coefficient. Diamonds represent steady-state solution; m=1. Rectangles represent transient solution at long time; m=1. Triangles represent steady-state solution; m=10. Ovals represent transient solution at long time; m=10. $\hat{L} = 2.54 \times 10^{-2}$ cm. Note that $k_s = 0.409$ when m=1; and 3.32×10^{3} when m = 10 (where k_s is defined as in Eq.(23), with $\hat{D}_0$ replacing $\hat{D}$; the dimensionless analogue of Eq.(29) is $-D\partial C/\partial z = k_s C$).

Having confirmed the validity of our analysis, we proceeded to simulate the early behavior of permeation of DIMP in Neoprene membranes, as was first attempted - and described earlier in this report - using the 2-dimensional model with constant $\hat{D}$. In particular, we were seeking an explanation for experimental results indicating an anomalous dependence upon barrier thickness, $\hat{L}$, of the breakthrough time, $\hat{t}_B$, defined by the cumulative permeation of 540 ng/cm^2. We now relax the constant $\hat{D}$ assumption by letting m vary between zero and ten, and setting $\hat{D}_0 = \frac{\hat{D}_i}{e^m}$ (see equation 29), where $\hat{D}_i$ is fixed at the value of the diffusion coefficient that has been used until now, which had been obtained from a separate immersion experiment [10]. Thus, equation (30) results in there being a lower diffusion coefficient, at any concentration, as m is increased.

We see (in figure 16) that, when m = 10, at breakthrough - as compared to steady-state (figure 15) - the dimensionless downstream concentration (C at z=1) is much lower (0.054). The corresponding steady-state value is 0.644. Thus, the effective diffusion coefficient at the downstream boundary is 5.90 x 10^{-12} cm^2/sec at breakthrough and 2.16 x 10^{-9} cm^2/sec at steady-state. For the same value of m (10), when the barrier thickness was increased from 2.54 x10^{-2} to 7.62 x 10^{-2} cm (10 to 30 mils), the concentration at z=1 at breakthrough, decreased from 0.054 to 0.0062. Thus, when $\hat{L}$ was tripled, $\hat{D}$ (at z=1, at breakthrough) decreased only from 5.90 x 10^{-12} cm^2/sec to 3.67 x 10^{-12} cm^2/sec. This was the qualitative effect anticipated when it was decided to introduce the concentration dependence of $\hat{D}$: as $\hat{L}$ increases, the effective $\hat{D}$ decreases, enhancing the sensitivity of breakthrough time to $\hat{L}$. However, because C (at z=1, at breakthrough) remained in the vicinity of zero, the quantitative effect was marginal. With lower values of m, effects are even smaller. Nonetheless, as described below, we examined the theoretical dependence of $\hat{t}_B$ on $\hat{L}$.

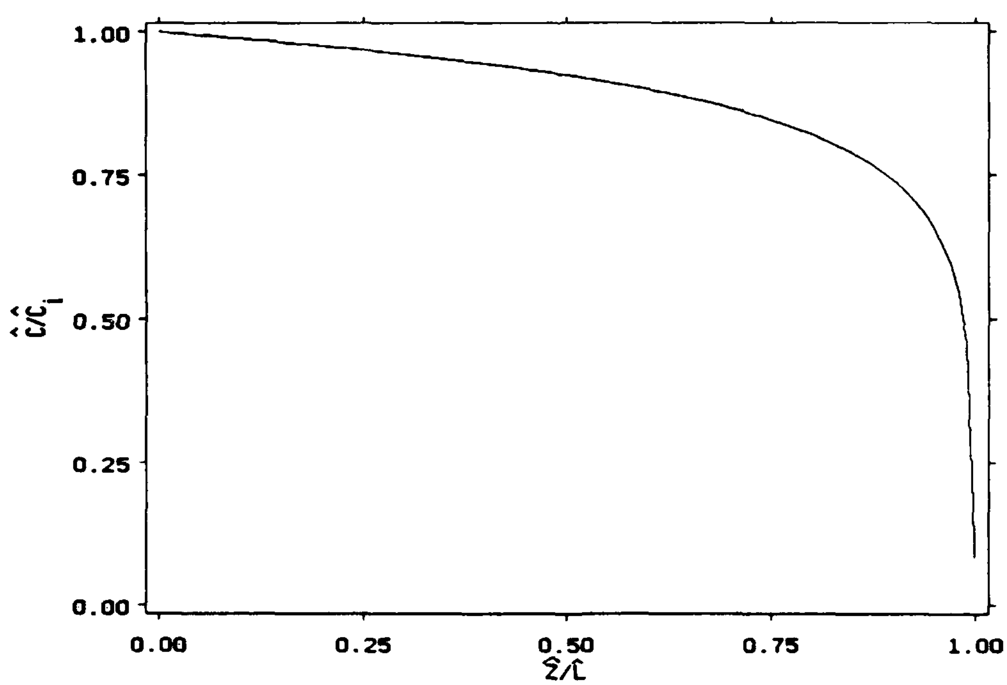

Figure 16. Breakthrough time dimensionless concentration profile; m=10. Parameters based on DIMP/Neoprene; $\hat{L}$ = 2.54 x 10^{-2} cm; k_s = 3.32 x 10^3.

A primary goal of this project remains the prediction of the relationship between breakthrough time, $\hat{t}_B$, and $\hat{L}$. Thus, an attempt was made to rationalize experimental data which had previously been shown [13] to be expressible by:

$$\hat{t}_B = \hat{K}\hat{L}^n \qquad (31)$$

where $\hat{K}$ and n are constants for a given barrier/penetrant system. In one set of computer runs, the parameters applied previously to simulate DIMP permeation in Neoprene with no upstream airflow (see section 2) were employed along with $\hat{L}$ values of 10 - 30 mils (2.54×10^{-2} - 7.62×10^{-2} cm), and $\hat{k}_s$ of either 4.52×10^{-7} or 4.52×10^{-8} cm/sec. The first $\hat{k}_s$ value is an estimated mass transfer coefficient; the second was chosen to examine the effect of increased mass transfer resistance.

Table 1 lists n values - obtained from least squares fits to the theoretically calculated $\hat{t}_B$ vs. $\hat{L}$ data - as they varied with m, with $\hat{k}_s$ fixed at the higher (estimated) value above. (Equation (31) did indeed provide a good fit.) The theoretical results are in striking contrast to those derived from the experimental data for DIMP (Table 2), which include n values ranging from 1.6 to 5.4 (1.8 to 5.4 with no upstream air flow; 1.6 to 4.2 with an air flow of 1 liter/min), for various barrier materials. The results obtained using the $\hat{k}_s$ value an order of magnitude lower were similar in that n never exceeded 2. Thus, the concentration dependence of $\hat{D}$ cannot explain the anoumalous dependence of $\hat{t}_B$ on $\hat{L}$. Interestingly, the experimental results for Neoprene with no air flow above (n=2.14) are close to the range of theoretical prediction. However, the much higher n values for some of the remaining materials remain an enigma.

Table 1: Results of least squares fit of n values (eq. 31) to breakthrough times calculated with different m values (eq. 30); based on estimated parameters for DIMP in Neoprene.

m	n
0	1.66
1	1.74
2	1.79
3	1.85
4	1.90
5	1.95
6	1.97
7	1.985
8	1.99
9	1.996
10	2.00

Table 2: Summary of n values derived from least squares fit of eq. 31 [13] to breakthrough time data for agent simulant DIMP [3]		
With no upper chamber air flow		With upper chamber air flow of 1l/min
Smithers Rubber	n	n
Butyl 0001	No permeation	No permeation
Neoprene 0005	2.14	1.69
Hydrin 0008	5.40	4.19
SBR 0011	2.29	>1.53
Natural rubber 0010	1.79	1.60
Vamac 0007	3.03	>1.91
Nitrile 0004	No test performed	2.54
Silicone 0003	No test performed	2.31

5.0 Conclusions.

Improvement in the fit of modelling results to experimental data, has been achieved by inclusion of downstream gas-phase mass transfer effects. However, there remain marked discrepancies between theory and observation in the case of early-time permeation behavior, leading up to the "breakthrough time":

i) The experimentally observed, pronounced delay in the onset of permeation remains irreconcilable with the model, even after including the downstream gas-phase mass transfer resistance, as well as a concentration-dependent penetrant diffusion coefficient in the barrier, and adjustment of droplet contact angle.

ii) Similarly, variation of model parameters - in particular, those governing concentration dependence of the diffusion coefficient - proved unsuccessful in replicating the experimentally observed variety of dependences of breakthrough time upon barrier thickness.

This leads us to conclude that either the experimental data - at least at early times - were not accuratcly measured; or physical phenomena - e.g., complications arising from the presence of chemical additives in as-received rubber samples, or a non-equilibrium time-dependent droplet contact angle (droplet spread) - are responsible for the observed dynamics of permeation. The immediate plan is to attempt to reproduce the anomalous experimental results for at least one penetrant/barrier material combination.

6.0 List of Notations

$\hat{A}$	Droplet exposed surface area.
$\hat{C}_0$	Equilibrium concentration at the droplet base.
C	Dimensionless concentration as defined in the appendix by equation (34)
$\hat{C}^V$	Vapor concentration.
$\hat{C}_e^V$	Equilibrium vapor concentration.
C^0	Finite-difference approximation for the intermediate value which arises from the implicit computation of C.
$\hat{D}$	Solvent diffusion coefficient.
D_{AB}	Gas phase diffusion coefficient.
$\hat{K}$	Proportionality constant.
$\hat{k}_d$	Mass transfer coefficient representing evaporation from the surface of the droplet.
k_d	Dimensionless mass transfer coefficient as defined by equation (39).
$\hat{k}_m$	Mass transfer coefficient representing convection from upstream barrier surface.
k_m	Dimensionless mass transfer coefficient as defined by equation (40).
$\hat{k}_s$	Mass transfercoefficient governing transfer of mass from downstream barrier surface to the sweep gas.
k_s	Dimensionless mass transfer coefficient as defined by equation (38).
$\hat{L}$	Barrier thickness.
$\hat{m}_d$	Initial droplet mass.
$\bar{P}$	Partial pressure.
$\hat{P}^V$	vapor pressure of the solvent penetrant which was diisopropyl methyl phosphonate.
P_t	Total pressure.
$\hat{q}_A$	Amount accumulated within the barrier.
q_A	Dimensionless amount accumulated within the barrier defined, in equation (44).
$\hat{q}_B$	Cumulative mass flow at the base of the droplet.
q_B	Dimensionless mass flow at the base of the droplet as defined by equation (42).
$\hat{q}_E$	Mass evaporated from surface of the droplet.
q_E	Dimensionless mass evaporated from surface of the droplet as defined by equation (43).
$\hat{q}_M$	Amount lost from unwet portion of the upstream membrane surface.

q_E Dimensionless mass evaporated from surface of the droplet as defined by equation (43).

$\hat{q}_M$ Amount lost from unwet portion of the upstream membrane surface.

q_M Dimensionless amount lost from the unwet portion of the upstream membrane as defined by eq (45).

$\hat{q}_P$ Amount permeated through the downstream surface.

q_P Dimensionless amount permeated through the downstream surface, as defined by eq (41).

$\hat{r}$ Radial coordinate.

r Defined as $\hat{r}/\hat{R}_0$

$\hat{R}(t)$ Time-varying droplet radius.

Re Reynold's number.

$\hat{R}_s$ Membrane radius.

R_s Dimensionless membrane radius as defined by eq (32).

Sc Schmidt number

Sh Sherwood number.

$\hat{t}$ Time.

t Dimensionless time.

t_B Breakthrough time.

$\hat{V}$ Droplet volume.

$\hat{V}_0$ Initial droplet volume.

$\hat{z}$ Distance from the upstream barrier surface.

z Define by equation (35).

α Defined after equation (76).

β Defined after equation (76).

θ Contact angle.

λ Defined following equation (46).

$\hat{\rho}$ Droplet density.

σ Defined by equation (37).

7.0 References.

1. A. P. Angelopoulos, J. H. Meldon and N. S. Schneider, "Numerical Simulation for the Permeation of Barrier Materials by Neat Liquid Droplets", MTL-TR 88-35, U.S. Army Materials Technology Laboratory, October 1988.

2. A. P. Angelopoulos, J. H. Meldon and N. S. Schneider (1987), "Analysis of Membrane Permeation from a Deposited Droplet", Journal of Membrane Science, **34**, 317-329.

3. D. P. Segers and R. B. Spafford, "Immersion and Permeation Testing of Chemical Agent Polymers," Southern Research Institute,MTL-TR 87-60, U.S. Army Materials Technology Laboratory, December 1987.

4. J. H. Meldon, G. Severe, A. F. Wilde and N. S. Schneider (1990), "Numerical Simulation of Permeation from a Deposited Droplet", CRDEC Scientific Conference on Chemical Defense Research, Edgewood, November 1990.

5. H. L. Frisch and A. Novick-Cohen (1985), "Diffusion from a Sessile Aerosol Droplet through a Membrane", Journal of Colloid and Interface Science, **104**, 285-287.

6. H. L. Frisch and H. Ogawa (1986), "Special Cases of Diffusion from a Sessile Droplet through a Membrane", Journal of Colloid and Interface Science, **3**, 283-285.

7. H. Pak and H. L. Frisch (1986), "Numerical Integration of Diffusion Equation for an Aerosol Droplet of a Neat Substance", Journal of Colloid and Interface Science, **4**, 270-272.

8. G. O. Williams, H. L. Frisch and H. Ogawa (1988), "Diffusion from a Polymer-Thickened, Sessile, Aerosol Droplet through a Membrane", Journal of Colloid and Interface Science, **123**, 448-455.

9. G. O. Williams and H. L. Frisch (1991), "Diffusion from Sessile Droplets Through Membranes", Journal of Statistical Physics, **63**, 1035-1037.

10. A. F. Wilde, "Immersion Tests with Decontaminants and Simulants", MTL-TR 89-48, U.S. Army Materials Technology Laboratory, June 1989

11. J. Crank, (1975), "The Mathematics of Diffusion", Oxford Press, second ed., London.

12. J. C. Jaeger and M. Clarke, (1945), " Numerical Results for some Problems on Conduction of Heat in Slabs with Various Surface Conditions", Philosophical magazine series 7, **38**, 1947.

13. A. F. Wilde, "Materials Testing, Standardization, and Associated Projects", (Progress Report Submitted to CRDEC, September 9, 1986).

14. R. E. Treybal (1980), "Mass Transfer Operations", McGraw-Hill Book Company, 3rd ed, New York.

15. R.H., Perry and C. H. Chilt. 's. (1973), "Chemical Engineers' Handbook," 5th Ed., McGraw-Hill, New York

16. D. W., Peaceman and H. H. Rachford (1955), " The Numerical Solution of Parabolic and Elliptic Differential equations," Journal of the Society for Industrial and Applied Mathematics, 3, 28-41.

17. B. Carnahan, H. A. Luther and J. O. Wilkes. (1969), " Applied Numerical Methods," John Wiley & Sons, New York.

17. B. Carnahan, H. A. Luther and J. O. Wilkes. (1969), " Applied Numerical Methods," John Wiley & Sons, New York.

18. D. U. Von Rosenberg (1971), " Methods For The Numerical Solution Of Partial Differential Equations," Elsevier Publishing Company Inc., second ed, New York.

19. G. D. Smith, (1979), " Numerical Solution of Partial Differential Equations: Finite Difference Methods" Oxford Univ. Press, second ed, London.

Appendix

8.0 Conversion to Dimensionless Variables

To identify key parameters and generalize the results, equations (1) - (18) were rewritten in terms of the following dimensionless variables:

$$R_s = \frac{\hat{R}_s}{\hat{R}_0} \quad (32)$$

$$R = \frac{\hat{R}}{\hat{R}_0} \quad (33)$$

$$C = \frac{\hat{C}}{\hat{C}_i} \quad (34)$$

$$z = \frac{\hat{z}}{\hat{L}} \quad (35)$$

$$t = \frac{\hat{D}\hat{t}}{\hat{L}^2} \quad (36)$$

$$\sigma = \frac{\hat{C}_i}{\rho} \quad (37)$$

$$k_s = \frac{\hat{k}_s\hat{L}}{\hat{D}} \quad (38)$$

$$k_d = \frac{\hat{k}_d\hat{C}^{V}_{e}\hat{L}}{\hat{D}\hat{C}_i} \quad (39)$$

$$k_m = \frac{\hat{k}_m\hat{C}^{V}_{e}\hat{L}}{\hat{D}\hat{C}_i} \quad (40)$$

$$q_P = \frac{\hat{q}_P}{\hat{m}_d} \quad (41)$$

$$q_B = \frac{\hat{q}_B}{\hat{m}_d} \tag{42}$$

$$q_E = \frac{\hat{q}_E}{\hat{m}_d} \tag{43}$$

$$q_A = \frac{\hat{q}_A}{\hat{m}_d} \tag{44}$$

$$q_M = \frac{\hat{q}_M}{\hat{m}_d} \tag{45}$$

$\hat{m}_d$ is the initial droplet mass.

Equation (1) becomes:

$$\frac{1}{\lambda^2}\frac{\partial C}{\partial t} = \frac{\partial^2 C}{\partial r^2} + \frac{1}{r}\frac{\partial C}{\partial r} + \frac{1}{\lambda^2}\frac{\partial^2 C}{\partial z^2} \tag{46}$$

where $\lambda = \hat{L}/\hat{R}_0$.

The initial and boundary conditions become:

$$C(r, z, 0) = 0 \qquad 0 \le r \le R_s \qquad 0 \le z \le 1 \tag{47}$$

$$C(r, 0, t) = 1 \qquad 0 \le r \le R(t) \qquad t \ge 0 \tag{48}$$

$$\frac{\partial C(r, 0, t)}{\partial z} = k_m C(r, 0, t) \qquad R(t) \le r \le R_s \qquad t \ge 0 \tag{49}$$

$$\frac{\partial C(r, 1, t)}{\partial z} = -k_s C(r, 1, t) \qquad 0 \le r \le R_s \qquad t \ge 0 \tag{50}$$

$$\frac{\partial C(R_s, z, t)}{\partial r} = 0 \qquad 0 \le z \le 1 \qquad t \ge 0 \tag{51}$$

$$\frac{\partial C(0, z, t)}{\partial r} = 0 \qquad 0 \le z \le 1 \qquad t \ge 0 \tag{52}$$

Furthermore, equations 11,12,14,15 and17 become, respectively:

$$q_B = -\frac{6\sigma\lambda}{g(\theta)}\int_0^t \int_0^{R(t)} \frac{\partial C(r, 0, t)}{\partial z} r\,dr\,dt \tag{53}$$

$$q_{ed} = \frac{3\sigma\lambda k_d}{\pi}\int_0^t R^2(t)\,dt \tag{54}$$

$$q_P = \frac{6\sigma\lambda k_s}{g(\theta)}\int_0^t\int_0^{R_s} C(r,1,t)\,rdrdt \tag{55}$$

$$q_M = \frac{6\sigma\lambda k_m}{g(\theta)}\int_0^t\int_{R(t)}^{R_s} C(r,0,t)\,rdrdt \tag{56}$$

$$q_A = \frac{6\sigma\lambda}{g(\theta)}\int_0^L\int_0^{R_s} C(r,z,t)\,rdrdz \tag{57}$$

The integrals were evaluated by applying Simpson's rule to the numerical values of C(r,z,t) which had been determined as described below.

9.0 Calculation of the Mass Transfer Coefficients

In order to obtain a representative value for k_s, we referred to the configuration of the liquid-droplet challenge permeation tests conducted at Southern Research Institute [3]. In these experiments, a cylindrical test cell was divided into upper and lower chambers by the permeation barrier. In the lower chamber, a Teflon insert was used to accelerate the air stream, thereby promoting gas-phase mass transfer (see figure 18). The volume of the lower chamber was 6 cm^3 without the Teflon, and 3.5 cm^3 with the Teflon inserted. The volume of the upper chamber was 16 cm^3.

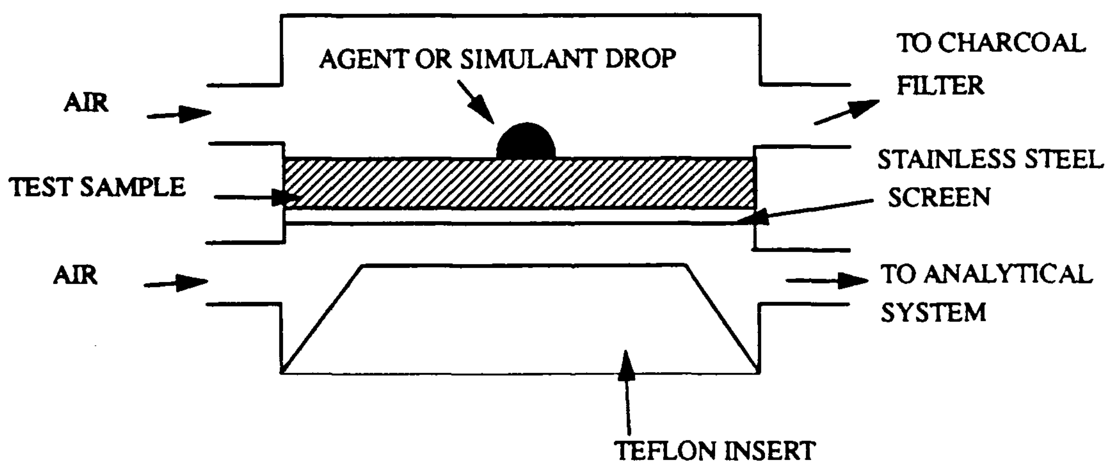

FIGURE 18. Experimental configuration of multichamber test cell [3]

The mass transfer coefficient at the bottom surface was obtained from the following correlation [14]:

$$Sh = 0.43 + 0.532 Re^{0.5} Sc^{0.3} \tag{58}$$

where Sh, the Sherwood number, is defined by:

$$Sh = \frac{k_G \bar{P} R T d}{D_{AB} P_t} \tag{59}$$

Re, the Reynolds number, is given by:

$$Re = \frac{\rho V d}{\mu} = \frac{\rho Q d}{\mu A} \tag{60}$$

and Sc, the Schmidt number, is given by:

$$Sc = \frac{\mu}{\rho D_{AB}} \tag{61}$$

In addition, Q=air flow rate, A= channel cross-sectional area of test cell, ρ=density of air, d= channel depth below sample, μ=viscosity of air, T=absolute temperature in Kelvin, R= ideal gas constant, P_t=absolute pressure in atmosphere, $\bar{P}$= partial pressure, k_G= gas phase mass transfer coefficient and for simplicity, carets (^) have been omitted above the symbols for dimensioned parameters. To estimate the Reynolds and the Schmidt numbers, we refer to the experimental conditions. Air at 25^0 C and 1 atmosphere was fed to the downstream chamber at 1000 ml/min. The cylindrical cell which contained the sample had a diameter of 3.57 cm., a height above each sample of 1.59 cm., and a depth below each sample of 1.27 cm. (see figure 19).

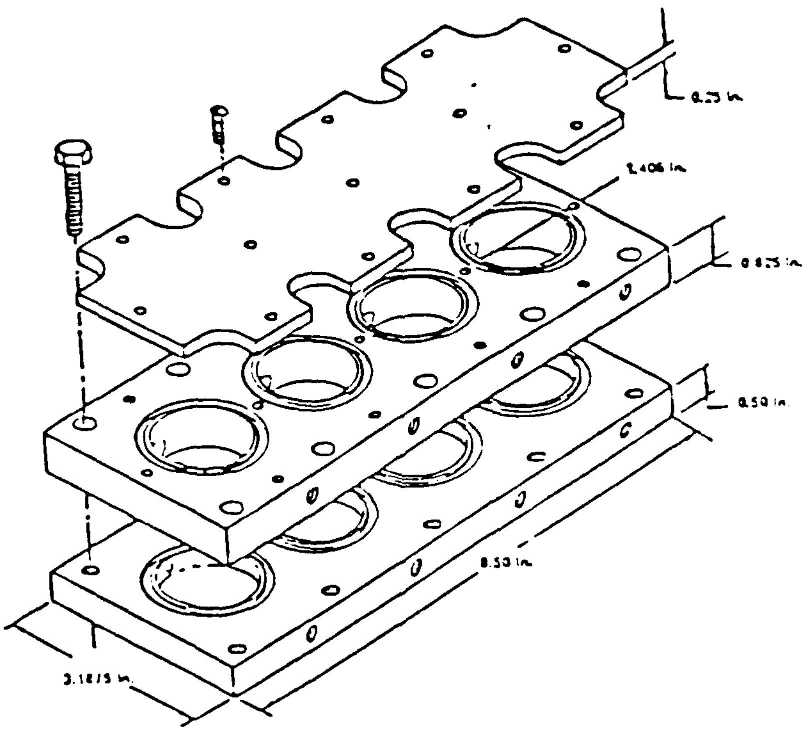

FIGURE 19. Multichamber test cell

The gas-phase diffusion coefficient (D_{AB}) was estimated using [15]

$$D_{AB} = \frac{10^{-3} T^{1.75} [(M_A + M_B) / (M_A M_B)]^{1/2}}{P [(\Sigma v)_A^{1/3} + (\Sigma v)_B^{1/3}]^2} \qquad (62)$$

where A and B were air and diisopropyl methyl phosphonate (DIMP), respectively, and:

M = molecular weight

v = atomic diffusion volume

D_{AB} was thereby estimated to be 6.34 x 10^{-2} cm^2/sec.

Once the Sherwood number was obtained, we derived the mass transfer coefficient $\hat{k}_G$ by rearranging eq (59) to:

$$\hat{k}_G = \frac{ShD_{AB}P_t}{RTD\bar{P}} \qquad (63)$$

The dimensionless expression for $\hat{k}_s$ is given by:

$$k_s = \frac{\hat{k}_s \hat{L}}{\hat{D}} \qquad (64)$$

where:

$\hat{k}_s$: the mass transfer coefficient defined by eq. (5), is equal to $\frac{\hat{k}_G \hat{P}^V}{\hat{C}_i}$

$\hat{L}$: thickness of the membrane.

$\hat{P}^V$: vapor pressure of the solvent penetrant, diisopropyl methyl phosphonate (DIMP), 0.27 mmHg.

$\hat{C}_i$: equilibrium dissolved concentration at the droplet base.

$\hat{D}$: diffusion coefficient of the solvent in the barrier material. Its value was obtained from separate immersion experiments [10].

The value for the gas-phase mass transfer coefficient above the unwet surface of the membrane, was calculated using:

$$\hat{k}_m = \frac{ShD_{AB}}{d} \qquad (65)$$

where the Sherwood number (Sh) and diffusion coefficient (D_{AB}) are estimated as before.

The mass transfer coefficient was made dimensionless as follows:

$$k_m = \frac{\hat{k}_m L \hat{C}_e^V}{\hat{D}\hat{C}_0} \tag{66}$$

where:

$\hat{C}_e^V$ is vapor concentration in equilibrium with the droplet, $\hat{P}^V/RT$.

In experiments with no air flow in the upper chamber of the test cell (see figure 18), the Reynolds number (Re) was set to zero (V=0 in equation 60), which gives a limiting value of 0.43 for the Sherwood number (Sh). Substitution of this value into equation 65, results in a mass transfer coefficient ($\hat{k}_m$) of 7.64 x 10^{-3} cm/sec. The corresponding dimensionless k_m (equation 66) was sufficiently close to zero (0.0170) to justify neglect of evaporation from the upstream surface. (Note, in addition, that $\hat{P}^V$ is so low as to justify neglect of the amount of mass lost from the droplet in saturating a closed upper chamber.)The same value (0.0170) was obtained for k_d.

10.0 Finite-Difference Approximation.

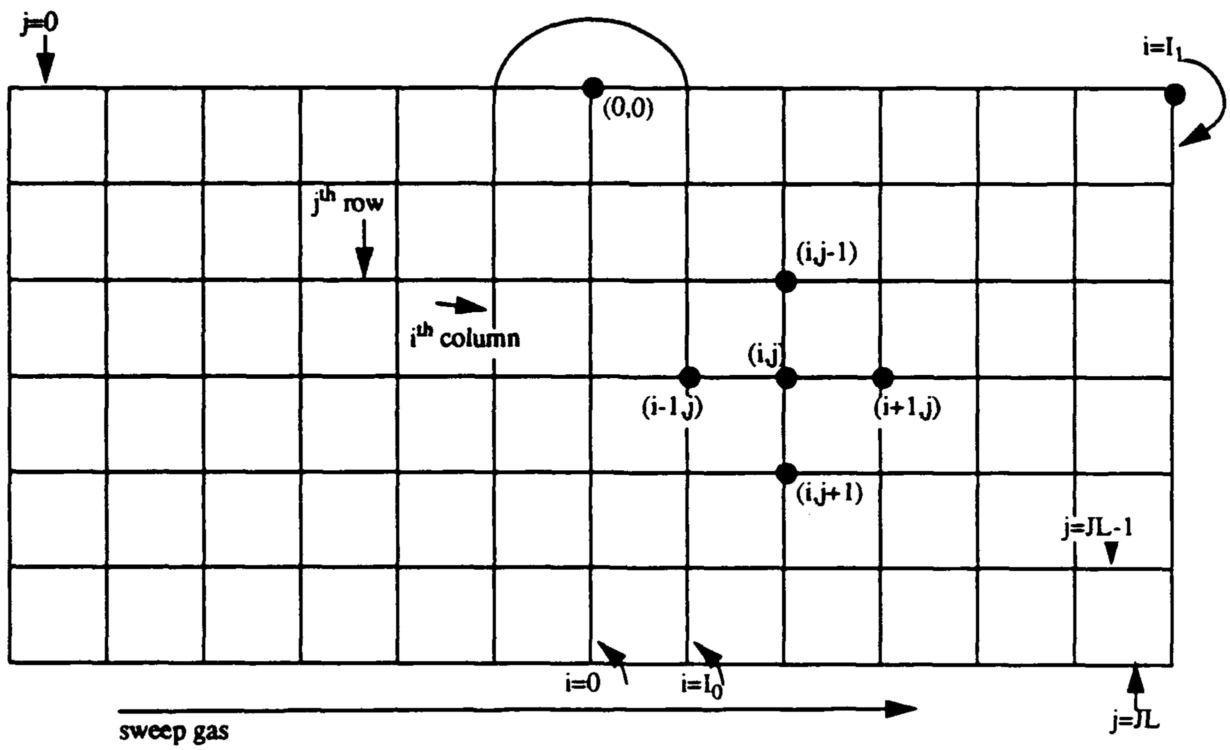

Figure 20. Arrangement of grid for finite difference analysis (note: grid is finer than shown; I_0 is not the grid point after 0)

The finite-difference method [16, 17, 18, 19] was used to obtain the concentration profile C(r,z,t) in the membrane. To solve the partial differential equation (46) governing concentration using the finite-difference technique, the membrane was first divided into grid-points (i,j), denoting space points having coordinates $i\Delta r$, $j\Delta z$. To minimize computation time, the implicit alternating-direction method developed by Peaceman and Rachford [14] was again used to obtain the numerical approximation for the concentration profile C(r,z,t).

The method consists of alternatively treating the respective spatial derivatives in the r and the z directions as unknowns in successive dimensionless time-steps $\Delta t/2$. The first half time-step is implicit in the r-direction, and the second half time-step is implicit in the z-direction [17]. The net result is the concentration C(r,z,t) at the end of interval Δt. If we denote the set of dimensionless concentrations at "old" time as $C_{i,j,n}$, those at the end of the first half time-step as $C^{\bullet}_{i,j}$, and the "new" values (at the end of interval Δt) as $C_{i,j,n+1}$, the finite-difference analogs to equation (46) become:

and
$$\frac{C^{\bullet}_{i,j} - C_{i,j,n}}{(\Delta t)/2} = \lambda^2\left(\frac{C^{\circ}_{i-1,j} - 2C^{\circ}_{i,j} + C^{\circ}_{i+1,j}}{(\Delta r)^2} + \frac{C^{\bullet}_{i+1,j} - C^{\bullet}_{i-1,j}}{2i(\Delta r)^2}\right) + \frac{C_{i,j-1,n} - 2C_{i,j,n} + C_{i,j+1,n}}{(\Delta z)^2} \tag{67}$$

$$\frac{C_{i,j,n+1} - C^{\bullet}_{i,j}}{(\Delta t)/2} = \lambda^2\left(\frac{C^{\bullet}_{i-1,j} - 2C^{\bullet}_{i,j} + C^{\bullet}_{i+1,j}}{(\Delta r)^2} + \frac{C^{\bullet}_{i+1,j} - C^{\bullet}_{i-1,j}}{2i(\Delta r)^2}\right) + \frac{C_{i,j-1,n+1} - 2C_{i,j,n+1} + C_{i,j+1,n+1}}{(\Delta z)^2} \tag{68}$$

Equations (67) and (68), plus the boundary conditions outlined below, each form a tridiagonal matrix of equations in terms of unknown concentrations. In order to obtain Table 3, equations 67 and 68 were used with $1 \le i \le I_1 - 1$ and $1 \le j \le jL + 1$. Due to the special boundary conditions (see next section) that exist at j=0 (z=0) and j=JL (z=1), and i = 0 (r=0) and i = I_1 (r=R_s) the tridiagonal matrix equations obtain by using equations (67) and (68) were not directly applicable at these positions. Separate matrices of equations were necessary in order to apply these boundary conditions. To solve the tridiagonal matrices in Tables 3 through 8, we used the Thomas algorithm [18].

10.1 Boundary Conditions.

At the unwet portion of the upper surface, i.e. j = 0, i>I_0 (see figure 20), boundary condition (49) applies. In the preceding report [1], a "symmetry" analog was used to eliminate the virtual concentration $C_{-1,j}$ in the finite difference approximation to the derivative in equation (49). However, that is justifiable only when $(\partial C/\partial z)$ is zero. Fortunately, that was generally true of the cases examined in that report. For greater generality, we employ the "quarter point" approach i.e., we write the partial differential equation at j=1/4, making the following approximation:

$$\left.\frac{\partial C}{\partial t}\right|_{i,j=1/4} = \frac{3}{4}\left.\frac{\partial C}{\partial t}\right|_{i,j=0} + \frac{1}{4}\left.\frac{\partial C}{\partial t}\right|_{i,j=1} \tag{69}$$

$$\left.\frac{\partial^2 C}{\partial r^2}\right|_{i,j=1/4} = \frac{3}{4}\left.\frac{\partial^2 C}{\partial r^2}\right|_{i,j=0} + \frac{1}{4}\left.\frac{\partial^2 C}{\partial r^2}\right|_{i,j=1} \tag{70}$$

$$\left.\frac{\partial C}{\partial r}\right|_{i,j=1/4} = \frac{3}{4}\left.\frac{\partial C}{\partial r}\right|_{i,j=0} + \frac{1}{4}\left.\frac{\partial C}{\partial r}\right|_{i,j=1} \tag{71}$$

$$\left.\frac{\partial^2 C}{\partial z^2}\right|_{i,j=1/4} \approx \frac{\left.\frac{\partial C}{\partial z}\right|_{i,j=1/2} - \left.\frac{\partial C}{\partial z}\right|_{i,j=0}}{\frac{\Delta z}{2}} \tag{72}$$

where:

$$\left.\frac{\partial C}{\partial z}\right|_{i,j=1/2} = \frac{C_{i,1} - C_{i,0}}{\Delta z} \tag{73}$$

and:

$$\left.\frac{\partial C}{\partial z}\right|_{i,j=0} = k_m C_{i,0} \tag{74}$$

(according to the boundary condition).

We substituted the above approximations in equation (46). What follow are the general equations for j=0, when $I_0 < i \le I_1$:

$$3\left(\frac{1}{2i} - 1\right) C^{*}_{i-1,0} + 6(1+\beta) C^{*}_{i,0} - 3\left(1 + \frac{1}{2i}\right) C^{*}_{i+1,0} = \left\{ \begin{array}{l} \left(1 - \frac{1}{2i}\right) C^{*}_{i-1,1} - 2(1+\beta) C^{*}_{i,1} + \left(1 + \frac{1}{2i}\right) C^{*}_{i+1,1} \\ + (8\alpha + 2\beta) C_{i,1,n} + [6\beta - 8\alpha(1 + k_m \Delta z)] C_{i,0,n} \end{array} \right\} \tag{75}$$

and

$$[6\beta + 8\alpha(1 + k_m \Delta z)] C_{i,0,n+1} - (8\alpha - 2\beta) C_{i,1,n+1} = \left\{ \begin{array}{l} 3\left(1 - \frac{1}{2i}\right) C^{*}_{i-1,0} + 6(\beta - 1) C^{*}_{i,0} + 3\left(1 + \frac{1}{2i}\right) C^{*}_{i+1,0} \\ + \left(1 - \frac{1}{2i}\right) C^{*}_{i-1,1} + 2(\beta - 1) C^{*}_{i,1} + \left(1 + \frac{1}{2i}\right) C^{*}_{i+1,1} \end{array} \right\} \tag{76}$$

where $\beta = \frac{1}{\lambda^2} \frac{(\Delta r)^2}{\Delta t}$ and $\alpha = \frac{1}{\lambda^2} \left(\frac{\Delta r}{\Delta z}\right)^2$

A further complication arises from the boundary condition at r=0 (i=0). Here th. indeterminate form 0/0 results for $\frac{1}{r}\frac{\partial C}{\partial r}$. However, by applying l'Hôpital's rule, $\frac{1}{r}\frac{\partial C}{\partial r}$ becomes $\frac{\partial^2 C}{\partial r^2}$. Therefore, at i=0 the partial differential equation becomes:

$$\frac{\partial C}{\partial t} = 2\lambda^2\frac{\partial^2 C}{\partial r^2} + \frac{\partial^2 C}{\partial z^2} \tag{77}$$

The finite-difference analogues to (77) at z=0 (j=0) (see figure 20) are then:

$$(6\beta + 12)\,\dot{C}_{0,0} - 12\dot{C}_{1,0} = -2(\beta + 2)\,\dot{C}_{0,1} + 4\dot{C}_{1,1} + [6\beta - 8\alpha(1 + k_m\Delta z)]\,C_{0,0,n} + 2(4\alpha + \beta)\,C_{0,1,n} \tag{78}$$

and

$$(2\beta - 8\alpha)\,C_{0,1,n+1} + [6\beta + 8\alpha(1 + k_m\Delta z)]\,C_{0,0,n+1} = 12\mathring{C}_{1,0} + (6\beta - 12)\,\mathring{C}_{1,1} + (2\beta - 4)\,\mathring{C}_{0,1} \tag{79}$$

At $i=I_1$ ($r=R_s$), $\frac{\partial C}{\partial r}$ is again =0. As result, here the finite-difference analogs to (46) are:

$$-6\dot{C}_{I_1-1,0} + 6(1 + \beta)\,\dot{C}_{I_1,0} = 2\dot{C}_{I_1-1,1} - 2(1 + \beta)\,\dot{C}_{I_1,1} + (2\beta + 8\alpha)\,C_{I_1,1,n} + [6\beta - 8\alpha(1 + k_m\Delta z)]\,C_{I_1,0,n} \tag{80}$$

and

$$[8\alpha(1 + k_m\Delta z) + 6\beta]\,C_{I_1,0,n+1} + (2\beta - 8\alpha)\,C_{I_1,1,n+1} = \left\{\begin{array}{c} 6\mathring{C}_{I_1-1,0} + 6(\beta - 1)\,\mathring{C}_{I_1,0} + 2\mathring{C}_{I_1-1,1} \\ + 2(\beta - 1)\,\mathring{C}_{I_1,1} \end{array}\right\} \tag{81}$$

As emphasized earlier, a different boundary condition is applied at j=jL (z=1) than that used in the previous report (see equation 50). In order to incorporate it into the finite-difference analysis, we again used the quarter point approach. Thus, the second partial derivative with respect to z is approximated as:

$$\left(\frac{\partial^2 C}{\partial z^2}\right)_{i,jL-1/4} = \frac{\left(\frac{\partial C}{\partial z}\right)_{i,jL} - \left(\frac{\partial C}{\partial z}\right)_{i,jL-1/2}}{\frac{\Delta z}{2}} \tag{82}$$

where:

$$\left(\frac{\partial C}{\partial z}\right)_{i,jL} = -k_s C_{i,jL} \tag{83}$$

(according to boundary condition (50)), and:

$$\left(\frac{\partial C}{\partial z}\right)_{i,jL-1/2} \approx \frac{C_{i,jL} - C_{i,jL-1}}{\Delta z} \tag{84}$$

The finite-difference analogues at j=jL (z=1) then become:

$$3\left(\frac{1}{2i} - 1\right) C^{\bullet}_{i-1,jL} + 6(1+\beta)\, C^{\circ}_{i,jL} - 3\left(\frac{1}{2i} + 1\right) C^{\circ}_{i+1,jL} = \left\{ \begin{array}{c} \left(1 - \frac{1}{2i}\right) C^{\bullet}_{i-1,jL-1} - 2(1+\beta)\, C^{\circ}_{i,jL-1} \\ + \left(\frac{1}{2i} + 1\right) C^{\circ}_{i+1,jL-1} + (8\alpha + 2\beta)\, C_{i,jL-1} \\ + \left[6\beta - 8\alpha(1 + k_s \Delta z)\right] C_{i,jL,n} \end{array} \right\} \tag{85}$$

for the first half time-step and:

$$(2\beta - 8\alpha)\, C_{i,jL-1,n+1} + \left[6\beta + 8\alpha(1 + k_s \Delta z)\right] C_{i,jL,n+1} = \left\{ \begin{array}{c} 3\left(1 - \frac{1}{2i}\right) C^{\bullet}_{i-1,jL} + 6(\beta - 1)\, C^{\bullet}_{i,jL} \\ + 3\left(\frac{1}{2i} + 1\right) C^{\bullet}_{i+1,jL} + \left(1 - \frac{1}{2i}\right) C^{\circ}_{i-1,jL-1} \\ + 2(\beta - 1)\, C^{\circ}_{i,jL-1} + \left(\frac{1}{2i} + 1\right) C^{\circ}_{i+1,jL-1} \end{array} \right\} \tag{86}$$

for the second half time-step.

The convection boundary condition (equation 50) applies over the entire downstream surface. Accordingly, equations (85) and (86) were applied at all values of i except at the end points (i=0 and i=I_1), where the appropriate boundary conditions (equation 51 and 52) were again applied. The result is:

$$(6\beta + 12)\, C^{\bullet}_{0,jL} - 12 C^{\bullet}_{0,jL} = \left\{ \begin{array}{c} -2(\beta + 2)\, C^{\bullet}_{0,jL-1} + 4 C^{\bullet}_{1,jL-1} + 2(4\alpha + \beta)\, C_{0,jL-1,n} \\ + \left[6\beta - 8\alpha(1 + k_s \Delta z)\right] C_{0,jL,n} \end{array} \right\} \tag{87}$$

$$-6 C^{\bullet}_{I_1-1,jL} + 6(\beta + 1)\, C^{\bullet}_{I_1,jL} = \left\{ \begin{array}{c} 2 C^{\bullet}_{I_1-1,jL-1} - 2(\beta + 1)\, C^{\bullet}_{I_1,jL-1} + (8\alpha + 2\beta)\, C_{I_1,jL-1,n} \\ + \left[6\beta - 8\alpha(1 + k_s \Delta z)\right] C_{I_1,jL,n} \end{array} \right\} \tag{88}$$

for the first half time-step, and:

$$(2\beta - 8\alpha)\, C_{0,jL-1,n+1} + [6\beta + 8\alpha\,(1 + k_s\Delta z)\,]\, C_{0,jL,n+1} = \left\{ \begin{array}{c} 12C^{\circ}_{1,jL} + (6\beta - 12)\, C^{\circ}_{0,jL} + 4C^{\circ}_{1,jL-1} \\ \\ + (2\beta - 4)\, C^{\circ}_{0,jL-1} \end{array} \right\} \qquad (89)$$

$$(2\beta - 8\alpha)\, C_{0,jL-1,n+1} + [6\beta + 8\alpha\,(1 + k_s\Delta z)\,]\, C_{l_1,jL} = \left\{ \begin{array}{c} 6C^{\circ}_{l_1-1,jL} + 6\,(\beta - 1)\, C^{\circ}_{l_1,jL} + 2C^{\circ}_{l_1-1,jL-1} \\ \\ + 2\,(\beta - 1)\, C^{\circ}_{l_1,jL-1} \end{array} \right\} \qquad (90)$$

for the second half time-step

11.0 One Dimensional Transport with Concentration dependent Diffusion Coefficient.

For the fully-wetted barrier with concentration-dependent $\hat{D}$, the dimensionless partial differential equation becomes:

$$\frac{\partial C}{\partial t} = D\frac{\partial^2 C}{\partial z^2} + \frac{\partial D}{\partial C}\left(\frac{\partial C}{\partial z}\right)^2 \qquad (91)$$

where $D = \frac{\hat{D}}{\hat{D}_0}$.

Since eq (91) is non-linear, we linearize it to become:

$$\frac{\partial C}{\partial t} \approx D^{\psi}\frac{\partial^2 C}{\partial z^2} + \left(\frac{\partial D}{\partial C}\right)^{\psi}\left(\frac{\partial C}{\partial z}\right)^{\psi}\frac{\partial C}{\partial z} \qquad (92)$$

where ψ denotes conditions at "old time" - i.e., at the start of a finite-difference time step. To arrive at the solution presented in Table 9, the finite-difference approach as described in the previous section was used. The principal change (other than in dimension) was that the boundary condition at j=jL was applied using the following variation of the 1/4 point approach:

$$\left(\frac{\partial C}{\partial z}\right)_{jL-1/4,n+1} \approx \left(\frac{\partial C}{\partial z}\right)_{jL,n+1} - \frac{1}{4}\Delta z\left(\frac{\partial^2 C}{\partial z^2}\right)_{jL-1/4,n+1} \qquad (93)$$

where:

$$\left(\frac{\partial C}{\partial z}\right)_{jL,n+1} = -\frac{k_s}{D^{\Psi}} C_{jL,n+1} \tag{94}$$

$$\left(\frac{\partial^2 C}{\partial z^2}\right)_{jL-1/4,n+1} \approx \frac{\left(\frac{\partial C}{\partial z}\right)_{jL,n+1} - \left(\frac{\partial C}{\partial z}\right)_{jL-1/2,n+1}}{\frac{\Delta z}{2}} \tag{95}$$

and:

$$\left(\frac{\partial C}{\partial z}\right)_{jL-1/2,n+1} = \frac{C_{jL,n+1} - C_{jL-1,n+1}}{\Delta z} \tag{96}$$

It follows that:

$$\left(\frac{\partial^2 C}{\partial z^2}\right)_{jL-1/4,n+1} \approx \frac{2D^{\Psi} C_{jL-1,n+1} - 2\,(k_s \Delta z + D^{\Psi})\, C_{jL,n+1}}{D^{\Psi} \Delta z^2} \tag{97}$$

Table 3: *2-Dimensional Analysis; Tridiagonal Matrix Equations for the First Time-Step (implicit in r only) with $j \neq 0$; $j \neq jl$ and $0 \leq i \leq I_1$.*

$i = 0$	$(2\beta + 4)\, C^{*}_{0,j} - 4C^{*}_{1,j}$	$= d_0$
$i = 1$	$(\frac{1}{2i} - 1)\, C^{*}_{0,j} + 2\,(1+\beta)\, C^{*}_{1,j} - (1 + \frac{1}{2i})\, C^{*}_{2,j}$	$= d_1$
$i = \ldots$	$(\frac{1}{2i} - 1)\, C^{*}_{i-1,j} + 2\,(1+\beta)\, C^{*}_{i,j} - (1 + \frac{1}{2i})\, C^{*}_{i+1,j}$	$= d_i$
$i = I_1 - 1$	$(\frac{1}{2i} - 1)\, C^{*}_{I_1-2,j} + 2\,(1+\beta)\, C^{*}_{I_1-1,j} - (1 + \frac{1}{2i})\, C^{*}_{I_1,j}$	$= d_{I_1}$
$i = I_1$	$-2C^{*}_{I_1-1,j} + 2\,(1+\beta)\, C^{*}_{I_1,j}$	$= d_{I_1}$

$$d_i = \alpha C_{i,j-1,n} + 2(\beta - \alpha) C_{i,j,n} + \alpha C_{i,j+1,n} \qquad \text{if } j \neq 0$$

$$d_i = (1 - \frac{1}{2i}) C^{\circ}_{i-1,1} - 2(1+\beta) C^{\circ}_{i,1} + (1 + \frac{1}{2i}) C^{\circ}_{i+1,1} + (8\alpha + 2\beta) C_{i,1,n} + [6\beta - 8\alpha(1 + k_m \Delta z)] C_{i,0,n}$$

$$\text{if } j = 0;\ i > I_0$$

Table 4: *2-Dimensional Analysis; Tridigonal Matrix Equations for the First Half Time-Step (implicit in r only) with j=0;* $I_0 < i \leq I_1$

$i = I_0 + 1$ $\qquad 6(1+\beta) C^{\circ}_{I_0+1,0} - 3(1 + \frac{1}{2i}) C^{\circ}_{I_0+2,0} = d_{I_0+1}$

$i = I_0 + 2$ $\qquad 3(\frac{1}{2i} - 1) C^{\circ}_{I_0+1,0} + 6(1+\beta) C^{\circ}_{I_0+2,0} - 3(1 + \frac{1}{2i}) C^{\circ}_{I_0+3,0} = d_{I_0+2}$

$i = \ldots$ $\qquad 3(\frac{1}{2i} - 1) C^{\circ}_{i-1,0} + 6(1+\beta) C^{\circ}_{i,0} - 3(1 + \frac{1}{2i}) C^{\circ}_{i+1,0} = d_i$

$i = I_1 - 1$ $\qquad 3(\frac{1}{2i} - 1) C^{\circ}_{I_1-2,0} + 6(1+\beta) C^{\circ}_{I_1-1,0} - 3(1 + \frac{1}{2i}) C^{\circ}_{I_1,0} = d_{I_1-1}$

$i = I_1$ $\qquad -6C^{\circ}_{I_1-1,0} + 6(1+\beta) C^{\circ}_{I_1,0} = d_{I_1}$

$$d_i = (1 - \frac{1}{2i}) C^{\circ}_{i-1,1} - 2(1+\beta) C^{\circ}_{i,1} + (1 + \frac{1}{2i}) C^{\circ}_{i+1,1} + (8\alpha + 2\beta) C_{i,1,n} + [6\beta - 8\alpha(1 + k_m \Delta z)] C_{i,0,n}$$

$$\text{for } i > I_0 + 1$$

$$d_{I_0+1} = d_i - 3(\frac{1}{2i} - 1) \qquad \text{for } i = I_0 + 1$$

$$d_{I_1} = 2C^{\circ}_{I_1-1,1} - 2(1+\beta) C^{\circ}_{I_1,1} + (2\beta + 8\alpha) C_{I_1,1} + [6\beta - 8\alpha(1 + k_m \Delta z)] C_{I_1,0} \qquad \text{for } i = I_1$$

$$d_0 = -2(\beta + 2) C^{\circ}_{i,1} + 4C^{\circ}_{i+1,1} + [6\beta - 8\alpha(1 + k_m \Delta z)] C_{i,0} + (8\alpha + 2\beta) C_{i,1} \qquad \text{for i=0}$$

Table 5: *2-Dimensional Analysis; Tridiagonal Matrix Equations for the First Half Time-Step (implicit in r only) with j=JL;* $0 \le i \le I_1$.

$i = 0$	$(6\beta + 12)\, C^{\circ}_{0,JL} - 12 C^{\circ}_{1,JL}$	$= d_0$
$i = 1$	$3\left(\frac{1}{2i} - 1\right) C^{\circ}_{0,JL} + 6\,(1+\beta)\, C^{\circ}_{1,JL} - 3\left(\frac{1}{2i} + 1\right) C^{\circ}_{2,JL}$	$= d_1$
$i = \ldots$	$3\left(\frac{1}{2i} - 1\right) C^{\circ}_{i-1,JL} + 6\,(1+\beta)\, C^{\circ}_{i,JL} - 3\left(\frac{1}{2i} + 1\right) C^{\circ}_{i+1,JL}$	$= d_i$
$i = I_1$	$-6 C^{\circ}_{I_1-1,JL} + 6\,(1+\beta)\, C^{\circ}_{I_1,JL}$	$= d_{I_1}$

$$d_0 = -2\,(\beta+2)\, C^{\circ}_{0,JL-1} + 4 C^{\circ}_{1,JL-1} + 2\,(4\alpha+\beta)\, C_{0,JL-1} + [6\beta - 8\alpha\,(1 + k_s \Delta z)]\, C_{0,JL}$$

$$d_i = \left(1 - \frac{1}{2i}\right) C^{\circ}_{i-1,JL-1} - 2\,(1+\beta)\, C^{\circ}_{i,JL-1} + \left(\frac{1}{2i} + 1\right) C^{\circ}_{i+1,JL-1} + (8\alpha + 2\beta)\, C_{i,JL-1} + [6\beta - 8\alpha\,(1 + k_s \Delta z)]\, C_{i,JL}$$

$$d_{I_1} = 2 C^{\circ}_{I_1-1,JL-1} - 2\,(\beta+1)\, C^{\circ}_{I_1,JL-1} + (8\alpha + 2\beta)\, C_{I_1,JL-1} + [6\beta - 8\alpha\,(1 + k_s \Delta z)]\, C_{I_1,JL}$$

Table 6: *2-Dimensional Analysis; Tridiagonal Matrix of Equations for the Second Time-Step (implicit in z) with $I_0 + 1 \le i \le I_1$ if $I_0 \ne 0$*

$j = 0$	$[6\beta + 8\alpha(1 + k_m \Delta z)]\, C_{i,0}$	$-(8\alpha - 2\beta)\, C_{i,1}$		$= \overset{\circ}{d}_0$
$j = 1$	$-\alpha C_{i,0,nn+1}$	$+2(\beta + \alpha)\, C_{i,1,n+1}$	$-\alpha C_{i,2,n+1}$	$= \overset{\circ}{d}_1$
$j = \ldots$	$-\alpha C_{i,j-1,n+1}$	$+2(\beta + \alpha)\, C_{i,j,n+1}$	$-\alpha C_{i,j+1,n+1}$	$= \overset{\circ}{d}_j$
$j = JL - 1$	$-\alpha C_{i,JL-2,n+1}$	$+2(\beta + \alpha)\, C_{i,JL-1,n+1}$	$-\alpha C_{i,JL}$	$= \overset{\circ}{d}_{JL-1}$

$$\overset{\circ}{d}_j = \left(1 - \frac{1}{2i}\right) \overset{\circ}{C}_{i-1,j} + 2(\beta - 1)\, \overset{\circ}{C}_{i,j} + \left(1 + \frac{1}{2i}\right) \overset{\circ}{C}_{i+1,j} \text{ for } i \ne I_1,\ i \ne 0\ \&\ j \ne 0$$

$$\overset{\circ}{d}_j = 2\overset{\circ}{C}_{I_1-1,j} + 2(\beta - 1)\, \overset{\circ}{C}_{I_1,j} \text{ for } i = I_1;\ j \ne 0$$

$$\overset{\circ}{d}_j = (2\beta - 4)\, \overset{\circ}{C}_{0,j} + 4\overset{\circ}{C}_{1,j} \text{ for } i = 0;\ j \ne 0$$

$$\overset{\circ}{d}_j = 6\overset{\circ}{C}_{i-1,0} + 6(\beta - 1)\, \overset{\circ}{C}_{i,0} + 2\overset{\circ}{C}_{i-1,1} + 2(\beta - 1)\, \overset{\circ}{C}_{i,1} \text{ for } i = I_1;\ j = 0$$

$$\overset{\circ}{d}_j = 12\overset{\circ}{C}_{1,0} + (6\beta - 12)\, \overset{\circ}{C}_{0,0} + 4\overset{\circ}{C}_{1,1} + (2\beta - 4)\, \overset{\circ}{C}_{0,1} \text{ for } i = 0;\ j = 0$$

$$\overset{\circ}{d}_j = 3\left(1 - \frac{1}{2i}\right) \overset{\circ}{C}_{i-1,0} + 6(\beta - 1)\, \overset{\circ}{C}_{i,0} + 3\left(1 + \frac{1}{2i}\right) \overset{\circ}{C}_{i+1,0} + \left(1 - \frac{1}{2i}\right) \overset{\circ}{C}_{i-1,1} + 2(\beta - 1)\, \overset{\circ}{C}_{i,1} + \left(1 + \frac{1}{2i}\right) \overset{\circ}{C}_{i+1,1}$$

$$\text{for } i \ne I_1,\ i \ne 0\ \&\ j = 0$$

Table 7: *2-Dimensional Analysis; Tridiagonal Matrix Equations for the Second Time-Step (implicit in z) with* $0 \le i \le I_1$ *and* $j = JL$

$j = JL$	$(2\beta - 8\alpha)\, C_{i,JL-1}$	$+\ [6\beta + 8\alpha\,(1 + k_s\Delta z)\,]\, C_{i,JL}$	$= \dot{d}_{JL}$

$$\dot{d}_{JL} = 3\,(1 - \frac{1}{2i})\,\dot{C}_{i-1,JL} + 6\,(\beta - 1)\,\dot{C}_{i,JL} + 3\,(\frac{1}{2i} + 1)\,\dot{C}_{i+1,JL} + (1 - \frac{1}{2i})\,\dot{C}_{i-1,JL-1} + 2\,(\beta - 1)\,\dot{C}_{i,JL-1}$$

$$+\ (\frac{1}{2i} + 1)\,\dot{C}_{i+1,JL-1} \qquad \text{for } i \ne 0 \ \&\ i \ne I_1$$

$$\dot{d}_{JL} = 12\dot{C}_{1,JL} + (6\beta - 12)\,\dot{C}_{0,JL} + 4\dot{C}_{1,JL-1} + (2\beta - 4)\,\dot{C}_{0,JL-1} \qquad \text{for } i=0$$

$$\dot{d}_{JL} = 6\dot{C}_{I_1-1,JL} + 6\,(\beta - 1)\,\dot{C}_{I_1,JL} + 2\dot{C}_{I_1-1,JL-1} + 2\,(\beta - 1)\,\dot{C}_{I_1,JL-1} \qquad \text{for } i=I_1$$

Table 8: *2-Dimensional Analysis; Tridiagonal Matrix of Equations for the Second Time-Step (implicit in z) for* $0 \le i \le I_0,\ j \ne 0$

$j = 1$	$-\alpha C_{i,0,n+1} + 2\,(\beta + \alpha)\,C_{i,1,n+1} - \alpha C_{i,2,n+1}$	$= \dot{d}_1$
$j = \ldots$	$-\alpha C_{i,j-1,n+1} + 2\,(\beta + \alpha)\,C_{i,j,n+1} - \alpha C_{i,j+1,n+1}$	$= \dot{d}_j$
$j = j - 2$	$-\alpha C_{i,j-3,n+1} + 2\,(\beta + \alpha)\,C_{i,j-2,n+1} - \alpha C_{i,j-1,n+1}$	$= \dot{d}_{j-2}$
$j = JL$	$(2\beta - 8\alpha)\,C_{i,JL-1} + [6\beta + 8\alpha\,(1 + k_s\Delta z)\,]\,C_{i,JL}$	$= \dot{d}_{jl}$

$$\overset{\bullet}{d}_j = (1-\frac{1}{2i})\overset{\bullet}{C}_{i-1,j} + 2(\beta-1)\overset{\circ}{C}_{i,j} + (1+\frac{1}{2i})\overset{\circ}{C}_{i+1,j} \qquad \text{for } 2 \le j \le j-1$$

$$\overset{\bullet}{d}_j = (2\beta-4)\overset{\circ}{C}_{0,j} + 4\overset{\bullet}{C}_{1,j} \qquad \text{for i=0}$$

$$\overset{\bullet}{d}_j = (1-\frac{1}{2i})\overset{\bullet}{C}_{i-1,j} + 2(\beta-1)\overset{\circ}{C}_{i,j} + (1+\frac{1}{2i})\overset{\circ}{C}_{i+1,j} + \alpha \qquad \text{for j=1}$$

$$\overset{\circ}{d}_{JL} = 3(1-\frac{1}{2i})\overset{\circ}{C}_{i-1,JL} + 6(\beta-1)\overset{\circ}{C}_{i,JL} + 3(\frac{1}{2i}+1)\overset{\circ}{C}_{I+1,JL} + (1-\frac{1}{2i})\overset{\circ}{C}_{i-1,JL} + 2(\beta-1)\overset{\circ}{C}_{i,JL-1}$$

$$+ (\frac{1}{2i}+1)\overset{\bullet}{C}_{i+1,JL-1} \qquad \text{for } j = JL \ \& \ i \neq 0$$

$$\overset{\bullet}{d}_{JL} = 12\overset{\bullet}{C}_{1,JL} + (6\beta-12)\overset{\bullet}{C}_{0,JL} + 4\overset{\bullet}{C}_{1,JL-1} + (2\beta-4)\overset{\circ}{C}_{0,JL-1} \qquad \text{for j=JL \& i=0}$$

Table 9: *Tridiagonal Matrix Equations For The One-dimensional Fully-Wetted Surface Model.*

j=1:

$$(2\lambda D^{\Psi}+1)C_{1,n+1} - \left[\frac{\lambda dD^{\Psi}}{4}(C_{2,n}-1) + \lambda D^{\Psi}\right]C_{2,n+1} = d_1$$

j=2:

$$\left[\frac{\lambda dD^{\Psi}}{4}(C_{3,n}-C_{1,n}) - \lambda D^{\Psi}\right]C_{1,n+1} + (1+2\lambda D^{\Psi})C_{2,n+1} - \left[\frac{\lambda dD^{\Psi}}{4}(C_{3,n}-C_{1,n}) + \lambda D^{\Psi}\right]C_{3,n+1} = d_2$$

j:

$$\left[\frac{\lambda dD^{\Psi}}{4}(C_{j+1,n}-C_{j-1,n}) - \lambda D^{\Psi}\right]C_{j-1,n+1} + (2\lambda D^{\Psi}+1)C_{j,n+1} -$$

$$\left[\frac{\lambda dD^{\Psi}}{4}(C_{j+1,n}-C_{j-1,n}) + \lambda D^{\Psi}\right]C_{j+1,n+1} = d_n$$

j=jL-1:

$$\left[\frac{\lambda dD^{\Psi}}{4}(C_{jL,n}-C_{jL-2,n})-\lambda D^{\Psi}\right]C_{jL-2,n+1}+(2\lambda D^{\Psi}+1)\,C_{jL-1,n+1}-$$
$$\left[\frac{\lambda dD^{\Psi}}{4}(C_{jL,n}-C_{jL-2,n})+\lambda D^{\Psi}\right]C_{jL,n+1} = d_{jL-1}$$

j=jL:

$$\left[1-8\lambda D^{\Psi}-2\Delta t dD^{\Psi}\left(\frac{k_s C_{jL,n}}{D^{\Psi}\Delta z}\right)\right]C_{jL-1,n+1}+[3+8\lambda\,(\Delta z k_s+D^{\Psi})\,]\,C_{jL,n+1}+$$
$$\left[2\Delta t dD^{\Psi}\frac{(k_s C_{jL,n})\;(k_s\Delta z+D^{\Psi}-2\Delta z k_s)}{(D^{\Psi^2}\Delta z)}\right]C_{jL,n+1} = d_{jL}$$

$$d_1 = C_{1,n}-\frac{\lambda D^{\Psi}}{4}(C_{2,n}-1)+\lambda D^{\Psi}$$

$$d_j = C_{j,n}$$

$$d_{jL} = C_{jL-1,n}+3C_{jL,n}$$

dD^{Ψ} is the derivative of D^{Ψ} with respect to C.

$$\lambda = \frac{\Delta t}{\Delta z^2}$$

12.0 Programs Listing.

12.1 2- Dimensional model

```
PROGRAM DRPEV
C
C   DROPLET DIFFUSION THROUGH A MEMBRANE (INCLUDING EVAPORATION)
C    FINITE-DIFFERENCE SOLUTION (IMPLICIT ALTERNATING DIRECTION METHOD)
C    SIMPSON'S RULE IS USED TO INTEGRATE OVER AREAS
C    TRIDAG: SUBROUTINE FOR SOLVING A TRIDIAGONAL SYSTEM OF SIMULTANEOUS
C     EQUATIONS.
C      CPRIME: VECTOR FOR TEMPORARY STORAGE OF CONCENTRATION COMPUTED BY TRIDAG
C    CSTAR: MATRIX OF CONCENTRATION C* AT THE END OF THE FIRST HALF TIME-STEP
C    IFREQ: NUMBER OF TIME-STEPS BETWEEN SUCCESSIVE PRINTING OF CONCENTRA-
C     TIONS.
C    AMS,BMS,CMS,EMS,FMS,GMS,AM,BM,CM,DM ARE THE COEFFICIENT VECTORS.
C
C     IMPLICIT DOUBLE PRECISION (A-H,O-Z)
      CHARACTER*15 FNAME
      REAL LAMBDA,KM,KD,KS,Q0,QACC,QT,QED
      DIMENSION AM(0:350),BM(0:350),CM(0:350),DM(0:350),C(0:350,0:350)
      DIMENSION CSTAR(0:350,0:350),CPRIME(0:350),AMS(0:350),BMS(0:350)
      DIMENSION CMS(0:350),EMS(0:350),FMS(0:350),GMS(0:350)
2     FORMAT(A)
      WRITE(*,100)
 100  FORMAT('INPUT FILE NAME FOR STORAGE OF CONC. PROFILE: ',$)
      READ(*,2)FNAME,QUEST
      OPEN(25,IOSTAT=IOS,ERR=79,FILE=FNAME,STATUS='NEW')
79    IF (IOS .NE. 0) WRITE(*,64) IOS
64    FORMAT('OPEN ERROR ',I4)
```

```
      WRITE(*,96)
96    FORMAT('INPUT FILE NAME FOR STORAGE OF DQDT: ',$)
      READ(*,2)FNAME
      OPEN(26,FILE=FNAME,STATUS='NEW',FORM='UNFORMATTED')
      WRITE(*,98)
98    FORMAT('INPUT FILE NAME FOR STORAGE OF Q/Q0: ',$)
      READ(*,2)FNAME
      OPEN(28,FILE=FNAME,STATUS='NEW',FORM='UNFORMATTED')
      WRITE(*,99)
99    FORMAT('INPUT FILE NAME FOR STORAGE OF R0: ',$)
      READ(*,2)FNAME
      OPEN(30,FILE=FNAME,STATUS='NEW',FORM='UNFORMATTED')
      WRITE(*,102)
102   FORMAT('INPUT FILE NAME FOR STORAGE OF QACC: ',$)
      READ(*,2)FNAME
      OPEN(32,FILE=FNAME,STATUS='NEW',FORM='UNFORMATTED')
      WRITE(*,104)
104   FORMAT('SHRINKING DROPLET RADIUS? (Y/N): ',$)
      READ(*,2) QUEST
      WRITE(*,105)
105   FORMAT('INPUT KM,KD,KS,THETA (deg.), SIGMA,AND LAMBDA: ',$)
      READ(*,*) KM,KD,KS,THETA,SIGMA, LAMBDA
      WRITE(*,107)
107   FORMAT('INPUT JL (even #), I0, I1(even #),IFIRST (mult.of 10)',
     &      /'AND ILAST (mult. of 10): ', $)
      READ(*,*) JL,I0, I1,IFIRST,ILAST
      WRITE(*,108)
108   FORMAT('INPUT DT AND IFREQ: ',$)
```

```
      READ(*,*)DT,IFREQ
        THETAR=2.0*3.1415926*THETA/360.0
        FTHETA=SIN(THETAR)*(2.0 + COS(THETAR))/(1.0 + COS(THETAR))**2
        INC=(ILAST-IFIRST)/10
        DZ=1.0/FLOAT(JL)
        DR=1.0/FLOAT(I0)
        RO=FLOAT(I1)/FLOAT(I0)
        R0=1
        ALPHA=(DR/DZ)**2/LAMBDA**2
        WRITE(25,110) KM,KD,KS,THETA,SIGMA,LAMBDA,RO,DR,DZ,IFIRST,ILAST,INC
110     FORMAT('UNSTEADY STATE DROPLET DIFFUSION IN A MEMBRANE, I.A.D.',
   &      ' METHOD, WITH PARAMETERS'// 'KM     = ', D10.5/ 'KD  = ',
   &       D10.5 /,'KS  = ',D10.5/,'THETA    = ', D10.5, ' deg. '/
   &      'SIGMA   = ', D10.5/ 'LAMBDA   = ',D10.5/ 'RO  = ', D10.5 /
   &      'DR    = ', D10.5/ ' DZ    = ',D10.5/ 'IFIRST  = ',I4
   &       / 'ILAST   =',I4/ 'INC    = ',I4)
        DO 10 I=0,I1
        DO 10 J=0,JL
        C(I,J)= 0
       CSTAR(I,J)= 0
10      CONTINUE
        DO 15  I=0,I0
        C(I,0) = 1
        CSTAR(I,0)=1
15      CONTINUE
      J0=1
      ICOUNT=0
      N=0
```

```
      T=0.0
      DQDT=0
      DQ0DT=0
      DQDTEM=0
      DQDTED=0
      Q=0
      QED=0
      QEM=0
      QACC=0
      Q0=0
      R0=1
18    BETA=DR**2/(DT*LAMBDA**2)
      AMS(0)=0.0
      BMS(0)=2.0*BETA + 4.0
      CMS(0)=-4.0
      DO 20 I=1,I1-1
      RI=I
      AMS(I)=1.0/(2.0*RI)-1.0
      BMS(I)=2.0*(1.0 + BETA)
      CMS(I)=-(1.0+1.0/(2.0*RI))
20    CONTINUE
      AMS(I1)=-2.0
      BMS(I1)=2.0*(1.0+BETA)
      CMS(I1)=0.0
      EMS(0)=0.0
      FMS(0)=6.0*(2.0+BETA)
      GMS(0)=-12.0
      DO 22 I=1,I1-1
```

```
      RI=I
        EMS(I)=3.0*(1.0/(2.0*RI)-1.0)
        FMS(I)=6.0*(1.0+BETA)
        GMS(I)=-3.0*(1.0+1.0/(2.0*RI))
22      CONTINUE
        EMS(I1)=-6.0
        FMS(I1)=6.0*(1.0+BETA)
        GMS(I1)=0.0
        DO 23 J=1,JL-1
        AM(J)=-ALPHA
        BM(J)=2.0*(ALPHA+BETA)
        CM(J)=-ALPHA
23      CONTINUE
        AM(0)=0.0
        BM(0)=6.0*BETA+8.0*ALPHA*(1.0+KM*DZ)
        CM(0)=2.0*BETA-8.0*ALPHA
        AM(JL)=2.0*BETA-8.0*ALPHA
        BM(JL)=6.0*BETA+8.0*ALPHA*(1.0+KS*DZ)
        CM(JL)=0.0
        IF (T .EQ. 0.0) GO TO 228
24      T=T+DT
        IF ( T .GT. (insert value)) GO TO 92
C       PREVIOUS LINE IS USED IN ORDER TO STOP COMPUTATION AFTER
C       THE NECESSARY DATA HAVE BEEN COMPUTED.
C
        N=N+1
        ICOUNT=ICOUNT + 1
        Q=Q + DQDT*DT/2.0
```

```
      Q0=Q0+DQ0DT*DT/2.0
            QED=QED + DQDTED*DT/2.0
            QEM=QEM + DQDTEM*DT/2.0
            IF (I0 .NE. -1) THEN
            DO 25 J=J0,JL-1
            DO 35 I=0,I1
            DM(I)=ALPHA*C(I,J-1)+2.0*(BETA-ALPHA)*C(I,J)+ALPHA*C(I,J+1)
35           CONTINUE
            CALL TRIDAG(0,I1,AMS,BMS,CMS,DM,CPRIME)
            DO 40 I=0,I1
            CSTAR(I,J)=CPRIME(I)
40           CONTINUE
25           CONTINUE
            J=JL
            DO 41  I=0,I1
            IF (I .EQ. 0) THEN
            DM(0)=-(4.0+2.0*BETA)*CSTAR(0,JL-1)+4.0*CSTAR(1,JL-1)+2.0*
     &      (4.0*ALPHA+BETA)*C(0,JL-1)+(6.0*BETA-8.0*ALPHA*
     &      (1.0+KS*DZ))*C(0,JL)
            ELSE
            IF(I .EQ. I1) THEN
            DM(I1)=2.0*CSTAR(I1-1,JL-1)-2.0*(1.0+BETA)*CSTAR(I1,JL-1)+
     &      (8.0*ALPHA+2.0*BETA)*C(I1,JL-1)+(6.0*BETA-8.0*
     &      ALPHA*(1.0+KS*DZ))*C(I1,JL)
            ELSE
            DM(I)=-AMS(I)*CSTAR(I-1,JL-1)-BMS(I)*CSTAR(I,JL-1)-CMS(I)*
     &      CSTAR(I+1,JL-1)+(8.0*ALPHA+2.0*BETA)*C(I,JL-1)+
     &      (6.0*BETA-8.0*ALPHA*(1.0+KS*DZ))*C(I,JL)
```

```
                    END IF
          END IF
41        CONTINUE
          CALL TRIDAG(0,I1,EMS,FMS,GMS,DM,CPRIME)
          DO 46 I=0,I1
          CSTAR(I,JL)=CPRIME(I)
46        CONTINUE
          J=0
          DO 45 I=I0+1,I1
           IF (I .EQ. I1) THEN
           DM(I1)=(6.0*BETA-8.0*ALPHA*(1.0+KM*DZ))*C(I1,0)+
     &        (2.0*BETA+8.0*ALPHA)*C(I1,1)+2.0*CSTAR(I1-1,1)-
     &        2.0*(1.0+BETA)*CSTAR(I1,1)
           ELSE
           DM(I)=(6.0*BETA-8.0*ALPHA-8.0*ALPHA*KM*DZ)*C(I,0)+
     &       2.0*BETA*C(I,1)+8.0*ALPHA*C(I,1)-AMS(I)*
     &       CSTAR(I-1,1)-BMS(I)*CSTAR(I,1)-CMS(I)*CSTAR(I+1,1)
           END IF
45        CONTINUE
           DM(I0+1)=DM(I0+1)-3.0*(1.0/(2.0*FLOAT(I0+1))-1.0)
           CALL TRIDAG(I0+1,I1,EMS,FMS,GMS,DM,CPRIME)
           DO 47  I=I0+1,I1
           CSTAR(I,0)=CPRIME(I)
47        CONTINUE
          END IF
          IF (I0 .EQ. -1) THEN
          DO 50 J=1,JL-1
           DO 48 I=0,I1
```

```
      DM(I)=ALPHA*C(I,J-1)+2.0*(BETA-ALPHA)*C(I,J)+
   &        ALPHA*C(I,J+1)
48          CONTINUE
           CALL TRIDAG(0,I1,AMS,BMS,CMS,DM,CPRIME)
           DO 49 I=0,I1
           CSTAR(I,J)=CPRIME(I)
49         CONTINUE
50         CONTINUE
           J=0
           DO 51 I=0,I1
           IF (I .EQ. 0) THEN
           DM(I)=4.0*CSTAR(1,1)-2.0*(BETA+2.0)*CSTAR(0,1)+
   &       (8.0*ALPHA+2.0*BETA)*C(0,1)+(6.0*BETA-8.0*
   &        ALPHA*(1.0+KM*DZ))*C(0,0)
           ELSE
        IF (I .EQ. I1) THEN
            DM(I1)=(2.0*BETA+8.0*ALPHA)*C(I1,1)+(6.0*BETA-8.0*
   &         ALPHA*(1.0+KM*DZ))*C(I1,0)+2.0*CSTAR(I1-1,1)-
   &         2.0*(1.0+BETA)*CSTAR(I1,1)
        ELSE
        DM(I)=(6.0*BETA-8.0*ALPHA*(1.0+KM*DZ))*C(I,0)+(8.0*
   &        ALPHA+2.0*BETA)*C(I,1)-AMS(I)*CSTAR(I-1,1)-
   &        BMS(I)*CSTAR(I,1)-CMS(I)*CSTAR(I+1,1)
       END IF
            END IF
51      CONTINUE
            CALL TRIDAG(0,I1,EMS,FMS,GMS,DM,CPRIME)
            DO 52 I=0,I1
```

```
      CSTAR(I,J)=CPRIME(I)
52  CONTINUE
    J=JL
    DO 53 I=0,I1
    IF (I .EQ. 0) THEN
    DM(0)=-(4.0+2.0*BETA)*CSTAR(0,JL-1)+4.0*CSTAR(1,JL-1)+2.0*
   &     (4.0*ALPHA+BETA)*C(0,JL-1)+(6.0*BETA-8.0*ALPHA*
   &     (1.0+KS*DZ))*C(0,JL)
    ELSE
    IF (I .EQ. I1) THEN
    DM(I1)=2.0*CSTAR(I1-1,JL-1)-2.0*(1.0+BETA)*CSTAR(I1,JL-1)+
   &     (8.0*ALPHA+2.0*BETA)*C(I1,JL-1)+(6.0*BETA-8.0*
   &     ALPHA*(1.0+KS*DZ))*C(I1,JL)
    ELSE
    DM(I)=-AMS(I)*CSTAR(I-1,JL-1)-BMS(I)*CSTAR(I,JL-1)-CMS(I)*
   &    CSTAR(I+1,JL-1)+(8.0*ALPHA+2.0*BETA)*C(I,JL-1)+(6.0*
   &    BETA-8.0*ALPHA*(1.0+KS*DZ))*C(I,JL)
    END IF
    END IF
53  CONTINUE
    CALL TRIDAG(0,I1,EMS,FMS,GMS,DM,CPRIME)
    DO 54 I=0,I1
    CSTAR(I,JL)=CPRIME(I)
54  CONTINUE
    END IF
    DO 60 I=I0+1,I1
    RI=I
    DO 55 J=1,JL-1
```

```
      IF( I .EQ. I1 ) THEN
       DM(J)=2.0*CSTAR(I-1,J)+2.0*(BETA-1.0)*CSTAR(I,J)
       ELSE
       IF (I .EQ. 0) THEN
         DM(J)=(2.0*BETA-4.0)*CSTAR(0,J)+4.0*CSTAR(1,J)
       ELSE
         DM(J)=(1.0 - 1.0/(2.0*RI))*CSTAR(I-1,J)+2.0*(BETA-1.0)*
   &          CSTAR(I,J)+(1.0 + 1.0 /(2.0*RI))*CSTAR(I+1,J)
       END IF
       END IF
55      CONTINUE
        J=0
          IF (I .EQ. I1) THEN
          DM(0)=6.0*CSTAR(I1-1,0)+6.0*(BETA-1.0)*CSTAR(I1,0)+2.0*
   &          CSTAR(I1-1,1)+2.0*(BETA-1.0)*CSTAR(I1,1)
         ELSE
         IF (I .EQ. 0) THEN
              DM(0)=12.0*CSTAR(1,0)+6.0*(BETA-2)*CSTAR(0,0)+4.0*
   &          CSTAR(1,1)+2.0*(BETA-2)*CSTAR(0,1)
        ELSE
               DM(0)=3.0*(1.0-1.0/(2.0*RI))*CSTAR(I-1,0)+6.0*(BETA-1)*
   &           CSTAR(I,0)+3.0*(1.0+1.0/(2.0*RI))*CSTAR(I+1,0)+
   &           (1.0-1.0/(2  *RI))*CSTAR(I-1,1)+2.0*(BETA-1.0)*
   &           CSTAR(I,1)+(1.0+1.0/(2.0*RI))*CSTAR(I+1,1)
        END IF
        END IF
        J=JL
        IF (I .EQ. 0) THEN
```

```
      DM(JL)=2.0*(3.0*BETA-6.0)*CSTAR(0,JL)+12.0*CSTAR(1,JL)+
     &     2.0*(BETA-2.0)*CSTAR(0,JL-1)+4.0*CSTAR(1,JL-1)
      ELSE
      IF (I .EQ. I1) THEN
      DM(JL)=6.0*CSTAR(I1-1,JL)+6.0*(BETA-1.0)*CSTAR(I1,JL)+
     &     2.0*CSTAR(I1-1,JL-1)+2.0*(BETA-1.0)*CSTAR(I1,JL-1)
      ELSE
      DM(JL)=3.0*(1.0-1.0/(2.0*RI))*CSTAR(I-1,JL)+6.0*(BETA-1.0)*
     &     CSTAR(I,JL)+3.0*(1.0/(2.0*RI)+1.0)*CSTAR(I+1,JL)+
     &     (1.0-1.0/(2.0*RI))*CSTAR(I-1,JL-1)+2.0*(BETA-1.0)*
     &     CSTAR(I,JL-1)+(1.0/(2.0*RI)+1.0)*CSTAR(I+1,JL-1)
      END IF
      END IF
      CALL TRIDAG(0,JL,AM,BM,CM,DM,CPRIME)
      DO 61 J=0,JL
      C(I,J)=CPRIME(J)
61    CONTINUE
60    CONTINUE
      IF (I0 .EQ. -1) GO TO 220
      DO 75  I=0,I0
        RI=I
        DO 70 J=1,JL-1
      IF (I .EQ. 0)  THEN
         DM(J)=(2.0*BETA-4.0)*CSTAR(0,J)+4.0*CSTAR(1,J)
         ELSE
     DM(J)=(1.0-1.0/(2.0*RI))*CSTAR(I-1,J)+2.0*(BETA-1.0)*
     &        CSTAR(I,J)+(1.0 + 1.0/(2.0*RI))*CSTAR(I+1,J)
         END IF
```

```
70    CONTINUE
      J=JL
      IF (I .EQ. 0) THEN
       DM(JL)=12.0*CSTAR(1,JL)+2.0*(3.0*BETA-6.0)*CSTAR(0,JL)+4.0*
     &        CSTAR(1,JL-1)+2.0*(BETA-2.0)*CSTAR(0,JL-1)
      ELSE
       DM(JL)=3.0*(1.0-1.0/(2.0*RI))*CSTAR(I-1,JL)+6.0*(BETA-
     &        1.0)*CSTAR(I,JL)+3.0*(1.0/(2.0*RI)+1.0)*
     &        CSTAR(I+1,JL)+(1.0-1.0/(2.0*RI))*CSTAR(I-1,JL-1)+
     &        2.0*(BETA-1.0)*CSTAR(I,JL-1)+(1.0/(2.0*RI)+1.0)*
     &        CSTAR(I+1,JL-1)
       END IF
      DM(1)=DM(1) + ALPHA
      CALL TRIDAG(1,JL,AM,BM,CM,DM,CPRIME)
      DO 75 J=1,JL
      C(I,J)=CPRIME(J)
75    CONTINUE
C
C        FLOW THROUGH THE MEMBRANE SURFACE AT Z=1
C
220    SUM2=0
       SUM3=0
       DO 225 I=1,I1-1,2
       SUM2=SUM2+C(I,JL)*FLOAT(I)
225    CONTINUE
       DO 259 I=2,I1-2,2
       SUM3=SUM3+C(I,JL)*FLOAT(I)
259    CONTINUE
```

```
      AREA=DR**2/3.0*(C(0,JL)*FLOAT(0)+4.0*SUM2+2.0*SUM3+C(I1,JL)*
     & FLOAT(I1))
      DQDT=2.0*3.1415926*KS*LAMBDA*AREA
      Q=Q+DQDT*DT/2.0
C
C     ACCUMULATION WITHIN MEMBRANE
C
      SUM2=0
      DO 270 J=0,JL,2
      SUMR2=0
      SUMR3=0
      DO 260 I=1,I1-1,2
      SUMR2=SUMR2+C(I,J)*FLOAT(I)
 260  CONTINUE
      DO 262 I=2,I1-2,2
      SUMR3=SUMR3+C(I,J)*FLOAT(I)
 262  CONTINUE
      AREA=DR**2/3.0*(4.0*SUMR2+2.0*SUMR3+C(I1,J)*FLOAT(I1))
      IF ( J .EQ. 0 ) THEN
      AREA0=AREA
      ELSE
      IF ( J .EQ. JL ) THEN
      AREAJL=AREA
      ELSE
      SUM2=SUM2+AREA
      END IF
      END IF
 270  CONTINUE
```

```
      SUM3=0
      DO 271 J=1,JL-1,2
      SUMR2=0
      SUMR3=0
      DO 264 I=1,I1-1,2
      SUMR2=SUMR2+C(I,J)*FLOAT(I)
  264 CONTINUE
      DO 266 I=2,I1-2,2
      SUMR3=SUMR3+C(I,J)*FLOAT(I)
  266 CONTINUE
      AREA=DR**2/3.0*(4.0*SUMR2+2.0*SUMR3+C(I1,J)*FLOAT(I1))
      SUM3=SUM3+AREA
  271 CONTINUE
      VOLUME=DZ/3.0*(AREA0+4.0*SUM3+2.0*SUM2+AREAJL)
      QACC=2.0*3.1415926*LAMBDA*VOLUME
C
C     EVAPORATION FROM MEMBRANE SURFACE AT Z=0
C
      IF (KM .EQ. 0) GO TO 320
      M1=I1
      M0=0
      ADD=0
      IF (I0 .EQ. -1) GO TO 330
      M0=I0
      ET=FLOAT(I0)/2.0
      IET=ET
      IF (FLOAT(IET) .EQ. ET) GO TO 330
      M1=I1-1
```

```
C
      ADD=DR**2/2.0*(C(M1,0)+C(I1,0))*(FLOAT(M1)+0.5)
330   SUM2=0
      SUM3=0
      DO 325 I=M0+2,M1,2
      SUM2=SUM2+C(I-1,0)*FLOAT(I-1)
      IF (I .EQ. M1) GO TO 327
      SUM3=SUM3 + C(I,0)*FLOAT(I)
325   CONTINUE
327   AREA=DR**2/3.0*(C(M1,0)*FLOAT(M1)+4.0*SUM2+2.0*SUM3+C(M0,0)
    & *FLOAT(M0))
      AREA=AREA+ADD
      DQDTEM=2.0*3.1415926*KM*LAMBDA*AREA
      QEM=QEM+DQDTEM*DT/2.0
C
320   IF (I0 .EQ. -1) GO TO 228
      IF (I0 .NE. 0) GO TO 207
      I0=-1
      J0=0
      R0=0
      QED=QED+DQDTED*DT/2.0
      DQDTED=0
      GO TO 228
C
C     TOTAL FLOW INTO MEMBRANE
C
207   Q0=Q+QACC+QEM
C
```

```
C     EVAPORATION FROM DROPLET SURFACE
C
           DQDTED=KD*FTHETA*3.1415926*LAMBDA*R0**2
           QED=QED+DQDTED*DT/2.0
C
C     TOTAL FLOW FROM DROPLET (THIS IS USED AS A MATERIAL BALANCE CHECK)
C
           QT=Q0+QED
C
           IF (QUEST .EQ. 'N') GO TO 228
           DUM=3.0/(FTHETA*3.1415926)*QT*SIGMA
           IF (DUM .LE. 1.0) GO TO 211
           I0=-1
           J0=0
           R0=0
           DQDTED=0
           GO TO 228
211        RI0=(1.0-DUM)**(1.0/3.0)/DR
           R0=RI0*DR
           II0=RI0
           TI0=FLOAT(II0)+0.5
           I0P=II0
           IF (RI0 .GE. TI0) I0P=II0+1
           IF (I0P .GE. I0) GO TO 228
           I0=I0P
C
C
228        IF (ICOUNT .NE. IFREQ) GO TO 24
```

```
      ICOUNT=0
      WRITE(25,115)DT,T,DQDT,Q,Q0,QEM,QED,QACC,R0
115   FORMAT(//'DT    = ', D10.5
     &  //'AT A TIME T = ',D10.5/ 34X,'DQ/DT(OUT)  = ', D20.6/
     &  34X,'Q(OUT)   = ', D20.6 / 34X, 'Q(IN)  = ',D20.6 / 34X,
     &  'Q(EM)   = ',D20.6 / 34X, 'Q(ED)   = ', D20.6 / 34X,
     &  'Q(ACC)   = ' , D20.6 / 34X, 'R0   = ', D20.6 //
     &  'CONCENTRATIONS ARE'//)
      WRITE(26)T*2220.00,DQDT*44.98
C     THE VALUE THAT MULTIPLIED T IS THE FACTOR NECESSARY IN ORDER TO
C     CONVERT DIMENSIONLESS T INTO TIME IN MIN.  IT IS THE VALUE OF
C     L**2/(D*60). TO CONVERT DQDT INTO NG/SQ.CM.MIN WE HAD TO MULTIPLY
C     DIMENSIONLESS DQDT BY THE VALUE OBTAINED FROM (C0*R0**3*D)/L**2
C
      WRITE(28)T*2220.00,Q*100.00
C     THE SAME IS TRUE HERE FOR T. BUT Q WAS MULTIPLIED BY THE VALUE OBTAINED
C     FROM ((C0*R0**3)/10cm**2)*10*6 IN ORDER TO OBTAIN Q IN MICRO GRAM/SQ.CM
C
      DO 80 J=0, JL
      WRITE(25,120) (C(I,J), I=IFIRST, ILAST, INC)
120   FORMAT(10(D 10.4,2X),D10.4)
80    CONTINUE
C
C     THE FOLLOWING WAS DONE IN ORDER TO CHANGE THE TIME STEP DURING
C     COMPUTATION
C
      IF ( T .GT. 0.30 ) THEN
      DT=0.00005
```

```
      IFREQ=800
      GO TO 18
      ELSE
      IF ( T .GT. 0.05000 ) THEN
      DT=0.00001
      IFREQ=800
      GO TO 18
      END IF
      END IF
      GO TO 24
92    CLOSE (25,STATUS='KEEP')
      CLOSE (26,STATUS='KEEP')
      CLOSE (28,STATUS='KEEP')
      CLOSE (30,STATUS='KEEP')
      CLOSE (32,STATUS='KEEP')
      CLOSE (34,STATUS='KEEP')
      END
C
C
C
C
C
C
        SUBROUTINE TRIDAG(IF,L,A,B,C,D,V)
        DIMENSION A(0:350),B(0:350),C(0:350),D(0:350),V(0:350)
        DIMENSION BETA(0:350),GAMMA(0:350)
        BETA(IF)=B(IF)
        GAMMA(IF)=D(IF)/BETA(IF)
```

```
      IFP1=IF+1
        DO 5 I=IFP1,L
        BETA(I)=B(I)-A(I)*C(I-1)/BETA(I-1)
        GAMMA(I)=(D(I)-A(I)*GAMMA(I-1))/BETA(I)
5       CONTINUE
        V(L)=GAMMA(L)
        LAST=L-IF
        DO 10 K=1,LAST
        I=L-K
        V(I)=GAMMA(I)-C(I)*V(I+1)/BETA(I)
10      CONTINUE
        RETURN
        END
```

12.2 1- Dimensional Model

```
c     DIFFUSION IN A PLANE SHEET (ONE DIMENSIONAL ASPECT)
C     FINITE-DIFFERENCE METHOD (NON-LINEAR SOLUTION)
C     TRIDAG: SUBROUTINE FOR SOLVING A TRIDAGONAL SYSTEM OF
C     SIMULTANEOUS EQUATIONS
C     CPRIME: VECTOR FOR TEMPORARY STORAGE OF CONCENTRATION
C     COMPUTED BY TRIDAG
C     DSTAR:  DIFFUSION COEFFICIENT AT OLD TIME AS A FUNCTION
C     OF CONCENTRATION
C     DDSTAR: DERIVATIVE OF DSTAR
C     KS   : DIMENSIONLESS MASS TRANSFER COEFFICIENT
C     AM,BM,CM,DM ARE THE COEFFICIENT VECTORS.
C
      CHARACTER*20 FNAME
      REAL LAMBDA,KS,M
```

```
      double precision am,bm,cm,dm,c,cprime,dstar,ddstar
      DIMENSION AM(0:700),BM(0:700),CM(0:700),DM(0:700),
     & C(0:700),CPRIME(0:700),DSTAR(0:700),DDSTAR(0:700)
2     FORMAT(A)
      WRITE(*,100)
100   FORMAT('INPUT FILE NAME FOR CONC FILE: ',$)
      READ(*,2) FNAME
      OPEN(25,FILE=FNAME,STATUS='NEW')
      WRITE(*,101)
101   FORMAT('INPUT FILE NAME FOR DATA FILE: ',$)
      READ(*,2)FNAME
      OPEN(26,FILE=FNAME,STATUS='OLD')
      READ(26,*)KS,M,JL,JFIRST,JLAST
      READ(26,*)DT,IFREQ
      WRITE(*,90)
90    FORMAT('INPUT FILE NAME FOR STORAGE OF DQDT: ',$)
      READ(*,2)FNAME
      OPEN(27,FILE=FNAME,STATUS='NEW',FORM='UNFORMATTED')
      WRITE(*,91)
91    FORMAT('INPUT FILE NAME FOR STORAGE OF Q: ',$)
      READ(*,2)FNAME
      OPEN(28,FILE=FNAME,STATUS='NEW',FORM='UNFORMATTED )
C
      DZ=1.0/FLOAT(JL)
      INC=(JLAST-JFIRST)/10
      WRITE(25,102)KS,M,DT,JL,DZ,INC
102   FORMAT('KS= ',D10.5/'M= ',D10.5/'DT= ',D10.5/
     &     'JL= ',I4/'DZ= ',D10.5/'INC= ',I4//)
```

```
      DO 10 J=0,JL
      C(J)=0
      DSTAR(J)=EXP(M*C(J))
      DDSTAR(J)=M*EXP(M*C(J))
10    CONTINUE
      C(0)=1
      DSTAR(0)=EXP(M*C(0))
      DDSTAR(0)=M*EXP(M*C(0))
      ICOUNT=0
      N=0
      T=0.0
      DQDT=0.0
      Q=0.0
3     LAMBDA=DT/(DZ**2)
      IF (T .EQ. 0.0) THEN
      WRITE(25,103) T,LAMBDA
103   FORMAT('AT TIME T= ',D10.4,2X, 'LAMBDA= ',D10.4//
     &  'CONCENTRATIONS ARE'//)
      WRITE(25,104)(C(J),J=JFIRST,JLAST,INC)
104   FORMAT(10(D10.1,2X),D10.1)
      END IF
4     T=T+DT
      IF (Q .GT. (insert amount)) GO TO 92
C
C     PREVIOUS LINE IS USED IN ORDER TO STOP THE PROGRAM AFTER
C     COMPUTING DATA FOR A SPECIFIED Q OR T OR ...
C
      N=N+1
      ICOUNT=ICOUNT+1
```

```
      AM(1)=0.0
      BM(1)=1.0+2.0*LAMBDA*DSTAR(1)
      CM(1)=-(LAMBDA*DSTAR(1)+(LAMBDA/4.0)*(DDSTAR(1))*(C(2)-1.0))
      DO 15 J=2,JL-1
      AM(J)=-LAMBDA*DSTAR(J)+(LAMBDA/4.0)*(DDSTAR(J))*(C(J+1)-C(J-1))
      BM(J)=1.0+2.0*LAMBDA*DSTAR(J)
      CM(J)=-LAMBDA*DSTAR(J)-(LAMBDA/4.0)*(DDSTAR(J))*(C(J+1)-C(J-1))
15    CONTINUE
      AM(JL)=1.0-8.0*LAMBDA*DSTAR(JL)-2.0*DT*DDSTAR(JL)*
     & ((KS*C(JL))/(DSTAR(JL)*DZ))
        BM(JL)=3.0+8.0*LAMBDA*(DZ*KS+DSTAR(JL))+(2.0*DT*DDSTAR(JL)*
     &   KS*C(JL)*((KS*DZ+DSTAR(JL)-2.0*DZ*KS)/(DSTAR(JL)**2*
     &   DZ)))
      CM(JL)=0.0
      DO 16 J=1,JL
      IF(J .EQ. 1) THEN
       DM(1)=C(1)+LAMBDA*DSTAR(1)-(LAMBDA/4.0)*(DDSTAR(1))*(C(2)-1)
      ELSE
       IF (J .EQ. JL) THEN
        DM(JL)=C(JL-1)+3.0*C(JL)
       ELSE
       DM(J)=C(J)
       END IF
       END IF
16    CONTINUE
        CALL TRIDAG(1,JL,AM,BM,CM,DM,CPRIME)
          DO 17 J=1,JL
            C(J)=CPRIME(J)
17          CONTINUE
```

```
C     FLOW THROUGH MEMBRANE (AT Z=1).
C
      DQDT=KS*C(JL)
      Q=Q+DQDT*DT
C
        DO 20 J=1,JL
           DSTAR(J)=EXP(M*C(J))
           DDSTAR(J)=M*EXP(M*C(J))
20      CONTINUE
C
      IF (ICOUNT .NE. IFREQ) GO TO 4
      ICOUNT=0
       WRITE(25,105) DT,T,LAMBDA,DQDT,Q
105   FORMAT(//'DT= ',D15.5//'AT TIME T= ',D10.5/34X,'LAMBDA='
  &     ,D15.5/34X,'DQDT(OUT)= ',D15.5/34X,'Q(OUT)= ',D15.5
  &     //'CONCENTRATIONS ARE '//)
       WRITE(27)T,DQDT
       WRITE(28)T,Q
       WRITE(25,106)(C(J),J=JFIRST,JLAST,INC)
106    FORMAT(10(D10.4,2X),D10.4)
C
C     THE FOLLOWING LINES ARE USED IN ORDER TO CHANGE THE TIME
C     DURING COMPUTATION.
C
      IF(T .GT. 10.0) THEN
      DT=0.0001
      IFREQ=800
      GO TO 3
```

```
      ELSE
      IF (T .GT. 0.034) THEN
      DT=0.0000001
      IFREQ=1
      GO TO 3
      END IF
      END IF
      GO TO 4
92    CLOSE(25,STATUS='KEEP')
      CLOSE(26,STATUS='KEEP')
      CLOSE(27,STATUS='KEEP')
      CLOSE(28,STATUS='KEEP')
      END
C
C
C
C
      SUBROUTINE TRIDAG(IF,L,A,B,C,D,V)
      DOUBLE PRECISION A,B,C,D,V,BETA,GAMMA
      DIMENSION A(0:700),B(0:700),C(0:700),D(0:700),V(0:700)
      DIMENSION BETA(0:700),GAMMA(0:700)
      BETA(IF)=B(IF)
      GAMMA(IF)=D(IF)/BETA(IF)
      IFP1=IF+1
      DO 5 I=IFP1,L
      BETA(I)=B(I)-A(I)*C(I-1)/BETA(I-1)
      GAMMA(I)=(D(I)-A(I)*GAMMA(I-1))/BETA(I)
5     CONTINUE
```

```
      V(L)=GAMMA(L)
      LAST=L-IF
      DO 11 K=1,LAST
      I=L-K
      V(I)=GAMMA(I)-C(I)*V(I+1)/BETA(I)
11    CONTINUE
      RETURN
      END
```

DISTRIBUTION LIST

No. of Copies	To
	Commander, U.S. Army Chemical Research, Development, and Engineering Center, Aberdeen Proving Ground, MD 21010-5423
1	ATTN: SMCCR-DDE
1	SMCCR-DDD
1	SMCCR-DDP
1	SMCCR-HV
1	SMCCR-MSI
1	SMCCR-MU
1	SMCCR-MUC
1	SMCCR-MUP
1	SMCCR-NB
1	SMCCR-OPS (B. Eckstein)
1	SMCCR-OPF
1	SMCCR-OPP
1	SMCCR-OPR
1	SMCCR-PPC (W. Davis)
1	SMCCR-PPI (C. Groves)
1	SMCCR-PPI (S. Hughes)
1	SMCCR-PPI (T. Mitchell)
1	SMCCR-PPI (R. Lindsay)
1	SMCCR-PPI (LTC J.Andrighetti)
1	SMCCR-PPP
1	SMCCR-RS
1	SMCCR-RSC (E. Penski)
1	SMCCR-RSC-P
1	SMCCR-RSL
1	SMCCR-RSP
1	SMCCR-A (M. Miller)
1	SMCCR-RSP-B
1	SMCCR-RSP-P
1	SMCCR-RST
1	SMCCR-SF
1	SMCCR-SPS-T
1	SMCCR-ST
1	SMCCR-TDT (S. Lawhorne)
1	SMCCR-MUA (Record Copy)
	Commandant, U.S. Army Ordnance Missile and Munitions Center and School, Redstone Arsenal, AL 35897-6700
1	ATTN: ATSK-EI (Mr. Cranford)
	Commander, U.S. Army Missile Command, Redstone Scientific Information Center, Redstone Arsenal, AL 35898-5241
1	ATTN: AMSMI-RD-CS-R (Document Section)
1	AMSMI-ROC (Dr. B. Fowler)
	Commander, U.S. Army Missile Command, Redstone Arsenal, AL 35898-5500
1	ATTN: AMSMI-RGT (Mr. Maddix)
1	AMSMI-YDL, Bldg. 4505
1	AMSMI-YLP (Mr. N. C. Kattos)
	Commandant, U.S Army Chemical School, Fort McClellan, AL 36205-5020
1	ATTN: ATZN-CM
1	ATZN-CM-CC
1	ATZN-CM-CS
1	ATZN-CM-CT
1	ATZN-CM-MLB
1	ATZN-CM-NC
	Commander, U.S. Army Aviation Center, Fort Rucker, AL 36362-5000
1	ATTN: ATZQ-CAT-CA-M (CPT P. McCluskey)
1	ATZQ-D-MS
	Commander, U.S. Army Science and Technology Center, Far East Office, San Fransisco, CA 96328-5000
1	ATTN: AMXME-J-OP (David Baker)
1	AFDPRC/PR, Lowry Air Force Base, CO 80230-5000
	Director, Office of Environmental and Life Sciences, Office of the Under Secretary of Defense (R&E), The Pentagon, Washington, DC 20301-3080
1	ATTN: Mr. Thomas R. Dashiell
	Director, Defense Intelligence Agency, Washington, DC 20301-6111
1	ATTN: DT-5A (Mr. C. Clark)
1	HQDA, (DAMO-NCC), Washington, DC 20301-0403
1	HQ USAF/INKL, Washington, DC 20330-1550
	Commander, Naval Air Systems Command, Washington, DC 20361
1	ATTN: PMA 279A (B. Motsuk)
1	PMA 279C (LCDR F Smartt)
	Commander, Naval Sea Systems Command, Washington, DC 20362-5101
1	ATTN: Code 55X25
	Commander, Naval Sea Systems Command, Theater of Nuclear Warfare Program Office, Washington, DC 20362-5101
1	ATTN: Code TN20A (Dr. G. Patton)
	Commander, Naval Medical Command, Washington, DC 20372-5120
1	ATTN: MEDCOM-02C
	Commander, Naval Research Laboratory, 4555 Overlook Avenue, SW, Washington, DC 20375-5000
1	ATTN: Code 2526 (Library
1	Code 6182 (Dr. R. Taylor)
	Commanding Officer, Navy Intelligence Support Center, Washington, DC 20390
1	ATTN: NISC-633 (Collateral Library)
	Commanding General, Marine Corps Research, Development, and Acquisition Command, Washington, DC 20380-0001
1	ATTN: Code SSC NBC
1	Toxicology Information Center JH, 652 National Research Council, 2101 Constitution Avenue, NW, Washington, DC 20418
1	OSU Field Office, P.O. Box 1925, Eglin Air Force Base, FL 32542-1925
	Headquarters, Eglin Air Force Base, FL 32542-6008
1	ATTN: AD/YQO/YQX
1	USAFTAWC/THLO
1	Mr. L. Rodgers
	Commander, U.S. Army Infantry Center, Fort Benning, GA 31905-5273
1	ATTN: NBC Branch
1	Directorate of Plans and Training
1	Bldg. 2294
	Commandant, U.S. Army Infantry School, Fort Benning, GA 31905-5410
1	ATTN: ATSH-B, NBC Branch
1	ATSH-CD-CS-CS
	Commander, U.S. Army Infantry School, Fort Benning, GA 31905-5800
1	ATTN: ATSH-CD-MLS-C
	Commander, U.S. Army Armament, Munitions, and Chemical Command, Rock Island, IL 61299-6000
1	ATTN: AMSMC-ASN
1	AMSMC-IMP-L
1	AMSMC-IRA
1	AMSMC-IRD-T
1	AMSMC-SFS
	Director, U.S. Army Materiel Command, Field and Safety Activity, Charlestown, IN 47111-9669
1	ATTN: AMXOS-SE (Mr. W. P. Yutmeyer)

No. of Copies	To
	Commander, Naval Weapons Support Center, Crane, IN 47522-5050
1	ATTN: Code 5063 (Dr. J. R. Kennedy)
	Commander, U.S. Army TRADOC, Independent Evaluation Directorate, Fort Leavenworth, KS 66027-5130
1	ATTN: ATZL-TIE-C (Mr. C. Annett)
	Commander, U.S. Army Combined Arms Center Development Activity, Fort Leavenworth, KS 66027-5300
1	ATTN: ATZL-CAM-M
	Commander, U.S. Army Armor School, Fort Knox, KY 40121-5211
1	ATTN: ATZK-DPT (NBC School)
	Commander, U.S. Army Natick Research, Development, and Engineering Center, Natick, MA 01760-5010
1	ATTN: STRNC-AC
1	STRNC-UE
1	STRNC-WTS
1	STRNC-WT
1	STRNC-IC
1	STRNC-ICC
1	STRNC-IP
1	STRNC-ITP (Mr. Tassinari)
1	STRNC-YB
1	STRNC-YE
1	STRNC-YM
1	STRNC-YS
	Headquarters, Andrews Air Force Base, MD 20334-5000
1	ATTN: AFSC/SDTS
1	AFSC/SGB
	Commanding Officer, Naval Explosive Ordnance Disposal Technology Center, Indian Head, MD 20640-5070
1	ATTN: Code BC-2
1	Commander, Detachment S, USAG, Team III, Fort Meade, MD 20755-5985
	Commander, Harry Diamond Laboratories, 2800 Powder Mill Road, Adelphi, MD 20783-1145
1	ATTN: DELHD-RT-CB (Dr. Sztankay)
	Commander, U.S. Army Laboratory Command, 2800 Powder Mill Road, Adelphi, MD 20783-1145
1	ATTN: AMSLC-IM-TL
1	AMSLC-CT
	Director, U.S. Army Human Engineering Laboratory, Aberdeen Proving Ground, MD 21005-5001
1	ATTN: AMXHE-IS (Mr. Harrah)
	Project Manager, Smoke/Obscurants, Aberdeen Proving Ground, MD 21005-5001
1	ATTN: AMCPM-SMK-E (A. Van de Wal)
1	AMCPM-SMK-T
	Commander, U.S. Army Test and Evaluation Command, Aberdeen Proving Ground, MD 21005-5055
1	ATTN: AMSTE-TE-F
1	AMSTE-TE-T
	Director, U.S. Army Ballistic Research Laboratory, Aberdeen Proving Ground, MD 21005-5066
1	ATTN: SLCBR-OD-ST (Tech Reports)
	Director, U.S. Army Materiel Systems Analysis Activity, Aberdeen Proving Ground, MD 21005-5071
1	ATTN: AMXSY-GC (Mr. F. Campbell)
1	AMXSY-MO (Mr. H. Cohen)
	Commander, U.S. Army Toxic and Hazardous Materials Agency, Aberdeen Proving Ground, MD 21010-5401
1	ATTN: AMXTH-ES
1	AMXTH-TE

No. of Copies	To
	Commander, U.S. Army Environmental Hygiene Agency, Aberdeen Proving Ground, MD 21010-5422
1	ATTN: HSHB-O/Editorial Office
	Commander, U.S. Army Armament, Munitions, and Chemical Command, Aberdeen Proving Ground, MD 21010-5423
1	ATTN: AMSMC-HO (A) (Mr. J. K. Smart)
1	AMSMC-QAC (A)
1	AMSMC-QAE (A)
	Commander, U.S Army Technical Escort Unit, Aberdeen Proving Ground, MD 21010-5423
1	ATTN: AMCTE-AD
	Commander, U.S. Army Medical Research Institute of Chemical Defense, Aberdeen Proving Ground, MD 21010-5425
1	ATTN: SGRD-UV-L
	Director, Armed Forces Medical Intelligence Center, Building 1607 Fort Detrick, Frederick MD 21701-5004
1	ATTN: AFMIC-IS
	Commander, U.S. Army Medical Bioengineering Research and Development Laboratory, Fort Detrick, Frederick, MD 21701-5010
1	ATTN: SGRB-UBG (Mr. Eaton)
1	SGRS-UBG-AL, Bldg. 568
	Commander, HQ 1/163d ACR, MT, ARNG, 899 Parkway Lane, Billings, MT 59101-4652
1	ATTN: NBC (SFC W. G. Payne)
	Director, U.S. Army Research Office, P.O. Box 12211, Research Triangle Park, NC 27709-2211
1	ATTN: SLCRO-CB (Dr. R. Ghirardelli)
1	SLCRO-GS
	Commander, U.S. Army Cold Regions Research and Engineering Laboratory, Hanover, NH 03755-1290
1	ATTN: CRREL-RG
	Commander, U.S. Army Production Base, Modernization Activity, Dover, NJ 07801
1	ATTN: AMSMC-PBE-C(D)/Regber
	Commander, U.S. Army Armament Research, Development and Engineering Center, Picatinny Arsenal, NJ 07806-5000
1	ATTN: SMCAR-AE (S. Morrow)
1	SMCAR-AE (R. A. Trifiletti)
1	SMCAR-CCT
1	SMCAR-FSF-B
1	SMCAR-MSI
1	SMCAR-AET (Bldg. 335)
	Project Manager, Cannon Artillery Weapons Systems, Picatinny Arsenal, NJ 07806-5000
1	ATTN: AMCPM-CAWS-A
	Director, Los Alamos National Laboratory, Los Alamos, NM 87545
1	ATTN: (S. Gerstl) ADAL, Mail Stop A104
	Director, U.S. Army TRADOC Analysis Command, White Sands Missile Range, NM 88002-5502
1	ATTN: ATOR-TSL
1	ATOR-TDB (L. Dominquez)
	Commander/Director, U.S. Army Atmospheric Sciences Laboratory, White Sands Missile Range, NM 88002-5501
1	ATTN: SLCAS-AE (Dr. F. Niles)
1	SLCAS-AE-E (Dr. D. Snider)
1	SLCAS-AR (Dr. E. H. Holt)
1	SLCAS-AR-A (Dr. M. Heaps)
1	SLCAR-AR-P (Dr. C. Bruce)
1	SLCAR-AM (Dr. R. Sutherland)

No. of Copies	To
	Commander U.S. Army Materiel Command Science and Technology Center, Europe, APO, New York, NY 09079-4734
1	ATTN: AMXMI-E-OP (Joe Crider)
	Commander, Headquarters, 3d Ordnance Battalion, APO, New York, NY 09189-2737
1	ATTN: AEUSA-UH
	Commander, U.S. Military Academy, Department of Physics, West Point, NY 10996-1790
1	ATTN: Major Decker
	Headquarters, Wright Patterson AFB, OH 45433-6523
1	ATTN: WRDC/FIEEC
1	ASD/AESD
1	AAMRL/HET
1	FTD-TQTR, Wright Patterson AFB, OH 45433-6508
1	WRDC/FIES/SURVIAC, U.S. Air Force Research and Development Center, OH 45433-6553
1	AAMRL/TID, Wright Patterson AFB, OH 45433-6573
	Commandant, U.S. Army Field Artillery School, Fort Sill, OK 73503-5600
1	ATTN: ATSF-GA
	Commander, Naval Air Develoment Center, Warminster, PA 18974-5000
1	ATTN: Code 60332 (D. Herbert)
	Commandant, U.S. Army Academy of Health Sciences, Fort Sam, Houston, TX 78234-6100
1	ATTN: HSHA-CDH (Dr. R. H. Mosebar)
1	HSHA-CDS (CPT Eng)
1	HSHA-IPM
	Headquarters, Brooks AFB, TX 78235-5000
1	ATTN: HSD/RDTK
1	HSD/RDS
1	USAFSAM/VNC
	Commander, U.S. Army Dugway Proving Ground, Dugway, UT 84022-5010
1	ATTN: STEDP-SD (Dr. L. Salomon)
	Commander, U.S. Army Dugway Proving Ground, Dugway, UT 84022-6630
1	ATTN: STEDP-SD-TA-F (Technical Library)
	HQ Ogden Air Material Area, Hill AFB, UT 84056-5609
1	ATTN: MMWM
	Director, U.S. Army Communications-Electronics Command, Night Vision and Electro-Optics Directorate, Fort Belvoir, VA 22060-5677
1	ATTN: AMSEL-NV-D (Dr. R. Buser)
	Commander, Marine Corps Development and Education Command Quantico, VA 22134-5080
1	ATTN: Code D091, SPWT Section
	Deputy Director, Marine Corps Institute, Arlington, VA 22222-0001
1	ATTN: NBC CD; CDD2
	Commander, U.S. Army Nuclear and Chemical Agency, 7500 Backlick Road, Bldg. 2073, Springfield, VA 22150-3198
1	ATTN: MONA-CM
	Chief of Naval Research, 800 N. Quincy Street, Arlington, VA 22217
1	ATTN: Code 411
	Commander, U.S. Army Materiel Command, 5001 Eisenhower Avenue, Alexandria, VA 22333-0001
1	ATTN: AMCCN
1	AMCSF-C
1	AMCSCI
	Commander, Defense Technical Information Center, Cameron Station, Building 5, 5010 Duke Street, Alexandria, VA 22304-6145
2	ATTN: DTIC-FDAC
	Commander, Naval Surface Weapons Center, Dahlgren, VA 22448
1	ATTN: Code E4311
1	Code G51 (Brumfield)
	Commander, U.S. Army Foreign Science and Technology Center, 220 Seventh Street, NE, Charlottesville, VA 22901-5396
3	ATTN: A1FRTC, Gerald Schlesinger, Applied Technologies Branch
	Director, Aviation Applied Technology Directorate, Fort Eustis, VA 23604-5577
1	ATTN: SAVRT-ALT-ASV
	Commander, U.S. Army Training and Doctrine Command, Fort Monroe, VA 23651-5000
1	ATTN: ATCD-N
1	HQ, TAC/DRPS, Langely AFB, VA 23665-5001
	Commander, U.S. Army Logistics Center, Fort Lee, VA 23801-6000
1	ATTN: ATCL-MGF
	Commander, U.S. Army Armament, Munitions, and Chemical Command, Aberdeen Proving Ground, MD 21010-5423
1	ATTN: AMSMC-QAO-C(A) (Dr. P. Patel)
	Commander, U.S. Army Tank-Automotive Command, Warren, MI 48090
1	ATTN: AMSTA-NR (Mr. R. Case)
1	AMSTA-RTS (Mr. A. Pacis)
	U.S. Environmental Protection Agency, Woodbridge Avenue, (MS-104), Edison, NJ 08837-3679
1	ATTN: Exposure Reduction Technology Section (M. Gruenfeld)
1	Department of the Army, Aerostructures Directorate, MS-266, U.S. Army Aviation R&T Activity - AVSCOM, Langley Research Center, Hampton, VA 23665-5225
1	NASA - Langley Research Center, Hampton, VA 23665-5225
1	U.S. Army Propulsion Directorate, NASA Lewis Research Center 2100 Brookpark Road, Cleveland, OH 44135-3191
1	NASA - Lewis Research Center, 2100 Brookpark Road, Cleveland, OH 44135-3191
	Commander, Naval Weapons Center, China Lake, CA 93555
1	ATTN: Code 3647 (Materials Engineering Branch)
1	Code 3686 (GIDEP, ATTN: Richard Barr)
1	Code 3858 (Polymer Science Branch, ATTN: Dr. G. Lindsay)
	U.S. Army Materials Technology Laboratory, Watertown, MA 02172-0001
1	ATTN: SLCMT-TML
2	Authors

U.S. Army Materials Technology Laboratory
Watertown, Massachusetts 02172-0001
NUMERICAL SIMULATION OF PERMEATION FROM DEPOSITED DROPLETS: MODEL EXPANSION
Geralda Severe and Jerry H. Meldon

AD ______________
UNCLASSIFIED
UNLIMITED DISTRIBUTION

Key Words

Mathematical model
Barriers
Flux (rate)

Technical Report MTL TR 92-23, April 1992, 68 pp - illus-tables, D/A Project 1L162105AH84

A previoulsy published model of permeation from a droplet has been expanded. Effects of downstream mass transfer resistance and concentration dependence of the diffusion coefficient have been included. An attempt was made to fit experimental results for the permeation of di-iso-propyl-methyl-phosphonate (DIMP) through Neoprene and natural rubber. Simulated data do not reproduce the initial pronounced delay of experimental permeation. Furthermore, no rationale has been identified for the anonalous dependence of "breakthrough time" upon barrier thickness observed with several experimental systems.

U.S. Army Materials Technology Laboratory
Watertown, Massachusetts 02172-0001
NUMERICAL SIMULATION OF PERMEATION FROM DEPOSITED DROPLETS: MODEL EXPANSION
Geralda Severe and Jerry H. Meldon

AD ______________
UNCLASSIFIED
UNLIMITED DISTRIBUTION

Key Words

Mathematical model
Barriers
Flux (rate)

Technical Report MTL TR 92-23, April 1992, 68 pp - illus-tables, D/A Project 1L162105AH84

A previoulsy published *model of permeation from a droplet* has been expanded. Effects of downstream mass transfer resistance and concentration dependence of the diffusion coefficient have been included. An attempt was made to fit experimental results for the permeation of di-iso-propyl-methyl-phosphonate (DIMP) through Neoprene and natural rubber. Simulated data do not reproduce the initial pronounced delay of experimental permeation. Furthermore, no rationale has been identified for the anonalous dependence of "breakthrough time" upon barrier thickness observed with several experimental systems.

U.S. Army Materials Technology Laboratory
Watertown, Massachusetts 02172-0001
NUMERICAL SIMULATION OF PERMEATION FROM DEPOSITED DROPLETS: MODEL EXPANSION
Geralda Severe and Jerry H. Meldon

AD ______________
UNCLASSIFIED
UNLIMITED DISTRIBUTION

Key Words

Mathematical model
Barriers
Flux (rate)

Technical Report MTL TR 92-23, April 1992, 68 pp - illus-tables, D/A Project 1L162105AH84

A previoulsy published model of permeation from a droplet has been expanded. Effects of downstream mass transfer resistance and concentration dependence of the diffusion coefficient have been included. An attempt was made to fit experimental results for the permeation of di-iso-propyl-methyl-phosphonate (DIMP) through Neoprene and natural rubber. Simulated data do not reproduce the initial pronounced delay of experimental permeation. Furthermore, no rationale has been identified for the anonalous dependence of "breakthrough time" upon barrier thickness observed with several experimental systems.

U.S. Army Materials Technology Laboratory
Watertown, Massachusetts 02172-0001
NUMERICAL SIMULATION OF PERMEATION FROM DEPOSITED DROPLETS: MODEL EXPANSION
Geralda Severe and Jerry H. Meldon

AD ______________
UNCLASSIFIED
UNLIMITED DISTRIBUTION

Key Words

Mathematical model
Barriers
Flux (rate)

Technical Report MTL TR 92-23, April 1992, 68 pp - illus-tables, D/A Project 1L162105AH84

A previoulsy published model of permeation from a droplet has been expanded. Effects of downstream mass transfer resistance and concentration dependence of the diffusion coefficient have been included. An attempt was made to fit experimental results for the permeation of di-iso-propyl-methyl-phosphonate (DIMP) through Neoprene and natural rubber. Simulated data do not reproduce the initial pronounced delay of experimental permeation. Furthermore, no rationale has been identified for the anonalous dependence of "breakthrough time" upon barrier thickness observed with several experimental systems.